Biogeosciences

Long-chain diols in settling particles in tropical oceans: insights into sources, seasonality and proxies

Marijke W. de Bar[1], **Jenny E. Ullgren**[2], **Robert C. Thunnell**[†], **Stuart G. Wakeham**[3], **Geert-Jan A. Brummer**[4,5], **Jan-Berend W. Stuut**[4,5], **Jaap S. Sinninghe Damsté**[1,6], and **Stefan Schouten**[1,6]

[1]NIOZ Royal Netherlands Institute for Sea Research, Department of Marine Microbiology and Biogeochemistry, and Utrecht University, P.O. Box 59, 1790 AB Den Burg, Texel, the Netherlands
[2]Runde Environmental Centre, Runde, Norway
[3]Skidaway Institute of Oceanography, University of Georgia, 10 Ocean Science Circle, Savannah, USA
[4]NIOZ Royal Netherlands Institute for Sea Research, Department of Ocean Systems, and Utrecht University, P.O. Box 59, 1790 AB Den Burg, Texel, the Netherlands
[5]Vrije Universiteit Amsterdam, Faculty of Science, Department of Earth Sciences, De Boelelaan 1085, 1081HV Amsterdam, the Netherlands
[6]Department of Earth Sciences, Faculty of Geosciences, Utrecht University, Utrecht, the Netherlands
[†]deceased, 30 July 2018

Correspondence: Marijke W. de Bar (marijke.de.bar@nioz.nl)

Abstract. In this study we analyzed sediment trap time series from five tropical sites to assess seasonal variations in concentrations and fluxes of long-chain diols (LCDs) and associated proxies with emphasis on the long-chain diol index (LDI) temperature proxy. For the tropical Atlantic, we observe that generally less than 2 % of LCDs settling from the water column are preserved in the sediment. The Atlantic and Mozambique Channel traps reveal minimal seasonal variations in the LDI, similar to the two other lipid-based temperature proxies TEX$_{86}$ and U$_{37}^{K'}$. In addition, annual mean LDI-derived temperatures are in good agreement with the annual mean satellite-derived sea surface temperatures (SSTs). In contrast, the LDI in the Cariaco Basin shows larger seasonal variation, as do the TEX$_{86}$ and U$_{37}^{K'}$. Here, the LDI underestimates SST during the warmest months, which is possibly due to summer stratification and the habitat depth of the diol producers deepening to around 20–30 m. Surface sediment LDI temperatures in the Atlantic and Mozambique Channel compare well with the average LDI-derived temperatures from the overlying sediment traps, as well as with decadal annual mean SST. Lastly, we observed large seasonal variations in the diol index, as an indicator of upwelling conditions, at three sites: in the eastern Atlantic, potentially linked to Guinea Dome upwelling; in the Cariaco Basin, likely caused by seasonal upwelling; and in the Mozambique Channel, where diol index variations may be driven by upwelling from favorable winds and/or eddy migration.

1 Introduction

Several proxies exist for the reconstruction of past sea surface temperature (SST) based on lipids. The U$_{37}^{K'}$ is one of the most commonly applied proxies and is based on the unsaturation of long-chain alkenones (LCAs), which are produced by phototrophic haptophyte algae, mainly the cosmopolitan *Emiliania huxleyi* (Volkman et al., 1980; Brassell et al., 1986; Prahl and Wakeham, 1987; Conte et al., 1994). This index exhibits a strong positive correlation with SST (Müller et al., 1998; Conte et al., 2006). Another widely used organic paleotemperature proxy is the TEX$_{86}$, as originally proposed by Schouten et al. (2002), based on the relative distribution of archaeal membrane lipids, i.e., glycerol dialkyl glycerol tetraethers (GDGTs), which in the marine realm are mainly thought to be derived from the phylum Thaumarchaeota. Schouten et al. (2002) showed that the TEX$_{86}$ index mea-

sured in marine surface sediments is correlated with SST, and since then its application in paleoenvironmental studies has increased (see, e.g., review by Tierney, 2014). However, research has shown that despite their highest abundance being recorded in the upper 100 m of the water column, Thaumarchaeota can be present down to a depth of 5000 m (Karner et al., 2001; Herndl et al., 2005). Accordingly, GDGTs may be found in high concentrations below a depth of 100 m (e.g., Sinninghe Damsté et al., 2002; Wuchter et al., 2005), and several studies have indicated that TEX_{86} might be more reflective of subsurface temperatures in some regions (e.g., Huguet et al., 2007; Lopes dos Santos et al., 2010; Kim et al., 2012, 2015; Schouten et al., 2013; Chen et al., 2014; Tierney et al., 2017; see Zhang and Liu, 2018 for review).

Most recently a SST proxy based on the distribution of long-chain diols (LCDs), called the long-chain diol index, or LDI has been proposed (Rampen et al., 2012). This index is a ratio of 1,13- and 1,15-diols (i.e., alcohol groups at position C-1 and C-13 or C-15), and the analysis of globally distributed surface sediments has revealed that this index strongly correlates with SST. Since then, the index has been applied in several paleoenvironmental studies (e.g., Naafs et al., 2012; Lopes dos Santos et al., 2013; Jonas et al., 2017; Warnock et al., 2018). However, large gaps still remain in the understanding of this proxy. The largest uncertainty is that the main marine producer of LCDs is unknown. Although these diols have been observed in cultures of certain marine eustigmatophyte algae (e.g., Volkman et al., 1992, 1999; Méjanelle et al., 2003; Rampen et al., 2014b), the LCD distributions in cultures are different from those observed in marine sediments. Furthermore, Balzano et al. (2018) combined lipid analyses with 18S rRNA gene amplicon sequencing on suspended particulate matter (SPM) and did not find a significant direct correlation between LCD concentrations and sequences of known LCD-producers. Rampen et al. (2012) observed the strongest empirical relation between surface sediment-derived LDI values and SSTs for autumn and summer, suggesting that these are the main growth seasons of the source organisms. Moreover, the strongest correlation was also observed for the upper 20 m of the water column, suggesting that the LCDs are likely produced by phototrophic algae which thrive in the euphotic zone. Nevertheless, LDI temperatures based on surface sediments reflect an integrated signal of many years, which complicates the interpretation of the LDI in terms of seasonal production and depth of export production.

One way of resolving seasonality in the LCD flux and the LDI is to analyze time series samples from sediment traps that continuously collect sinking particles in successive time intervals over periods of a year or more. Such studies have been carried out for the $U_{37}^{K'}$ as well as for the TEX_{86} and associated lipids (e.g., Müller and Fischer, 2001; Wuchter et al., 2006; Huguet et al., 2007; Fallet et al., 2011; Yamamoto et al., 2012; Rosell-Melé and Prahl, 2013; Turich et al., 2013). However, very few studies have been undertaken for LCDs.

Villanueva et al. (2014) carried out a sediment trap study in Lake Challa (eastern Africa) and Rampen et al. (2008) in the upwelling region off Somalia. The latter study showed that 1,14-diols, produced by *Proboscia* diatoms strongly increased early in the upwelling season in contrast to 1,13- and 1,15-diols; thus they can be used to trace upwelling. However, neither of these sediment trap studies evaluated the LDI.
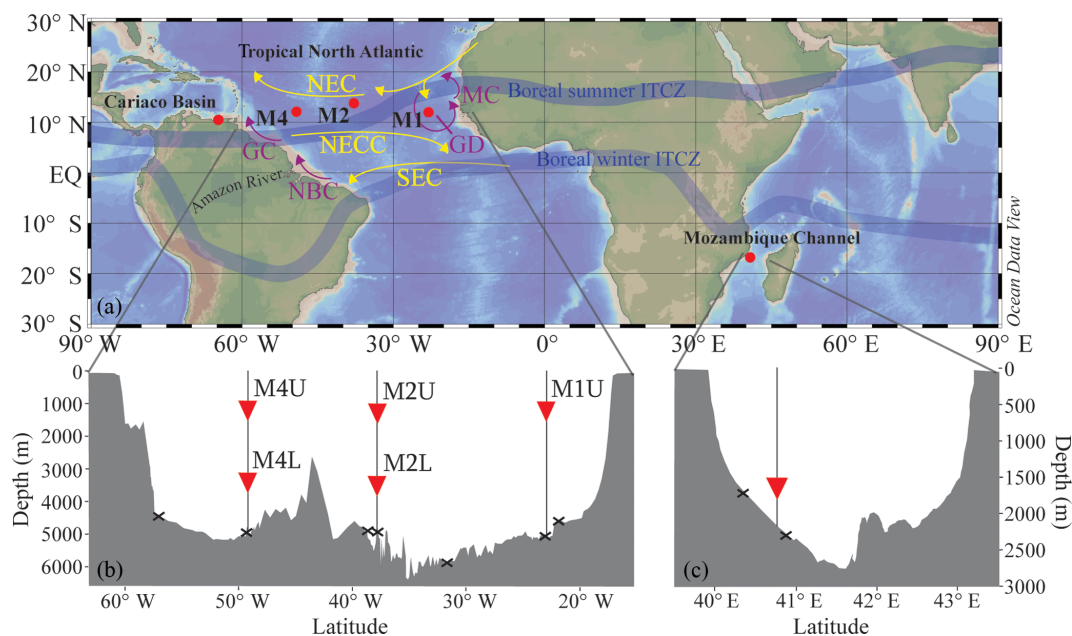
In this study, we assess seasonal patterns of the LDI for sediment trap series at five sites: in the Cariaco Basin, in the Mozambique Channel and three sites in the tropical North Atlantic. During this assessment, we compare the LDI values to satellite-derived SST, as well as results obtained for other temperature proxies, i.e., the TEX_{86}^H and $U_{37}^{K'}$. Moreover, for the Atlantic and Mozambique Channel, we compare the sediment trap proxy signals with those preserved in the underlying sediments, after settling and burial. Finally, we assess the applicability of the diol index, based on 1,14-diols produced by *Proboscia* diatoms (Sinninghe Damsté et al., 2003), as a tracer of upwelling and/or productivity in these regions.

2 Materials and methods

2.1 Study sites and sample collection

2.1.1 Tropical North Atlantic

The ocean current and wind patterns of the tropical Atlantic are mostly determined by the seasonal latitudinal shift of the intertropical convergence zone (ITCZ; Fig. 1). The ITCZ migrates southward during boreal winter, and northward during boreal summer. During summer, the southeast trade winds prevail, whereas during winter the northeast trade winds intensify. The northeast trade winds drive the North Equatorial Current (NEC) which flows westward. South of the NEC, the North Equatorial Countercurrent (NECC) flows towards the east (Stramma and Schott, 1999). The South Equatorial Current (SEC) flows westward and branches off in the North Brazil Current (NBC; Stramma and Schott, 1999). When the ITCZ is in the north, the NBC retroflects off the South American coast and is carried eastward into the NECC, and thus into the western tropical Atlantic (e.g., Richardson and Reverdin, 1987). North of the NBC, the Guiana Current (GC) disperses the outflow from the Amazon River towards the Caribbean Sea. (Müller-Karger et al., 1988, 1995). However, during boreal summer the NBC may retroflect, carrying the Amazon River plume far into the western Atlantic (e.g., Lefèvre et al., 1998; Coles et al., 2013). In fact, every late summer/autumn, the Amazon River outflow covers around 2×10^6 km^2 of the western North Atlantic, and the river delivers approximately half of all freshwater input into the tropical Atlantic (see Araujo et al., 2017, and references therein).

Figure 1. (a) Location map showing the five sediment trap mooring sites in the Cariaco Basin, the tropical North Atlantic (M1, M2 and M4) and the Mozambique Channel. Two of the moorings in the tropical North Atlantic (M2 and M4) contain an upper ("U") and a lower ("L") trap, shown in the bathymetric section below **(b)** with traps depicted as red triangles and surface sediments shown as black crosses. A similar section profile is shown for the Mozambique Channel **(c)**, where the sediment trap and the surface sediments are also indicated. All maps/sections were generated using Ocean Data View (Schlitzer, 2015). The approximate seasonal positions of the ITCZ are indicated, in addition to the North Equatorial Current (NEC), the North Equatorial Countercurrent (NECC), the South Equatorial Current (SEC), the Mauritania Current (MC), the Guinea Dome (GD), the North Brazil Current (NBC) and the Guiana Current (GC).

The eastern tropical North Atlantic is characterized by up-welling caused by the interaction between the trade winds and the movement of the ITCZ. Cropper et al. (2014) measured upwelling intensity along the northwest African coastline between 1981 and 2012, in terms of wind speed, SST and other meteorological data. They recognized three latitudinal zones: weak permanent annual upwelling north of 26° N, strong permanent upwelling between 21 and 26° N, and seasonal upwelling between 12 and 19° N related to the seasonal migration of the trade winds. Southeast of Cape Verde, large-scale cyclonic circulation forms the Guinea Dome (GD; Fig. 1), which centers around 10° N, 22° W (Mazeika, 1967), i.e., close to mooring site M1. The GD is a thermal upwelling dome, formed by near-surface flow fields associated with the westward NEC, the eastward NECC and the westward North Equatorial Undercurrent (NEUC) (Siedler et al., 1992). It forms a cyclonic circulation as a result of the eastward flow-ing NECC and the westward flowing NEC (Rossignol and Meyrueis, 1964; Mazeika, 1967). The GD develops from late spring to late fall due to the northern ITCZ position and the resulting Ekman upwelling, but shows significant interannual variability (Siedler et al., 1992; Yamagata and Iizuka, 1995; Doi et al., 2009) judging from general ocean circulation models. According to Siedler et al. (1992), upwelling is most intense between July and October when the ITCZ is in the GD region and the NECC is strongest.

At three sites, we analyzed five sediment trap series along a longitudinal transect in the North Atlantic ($\sim 12°$ N) to determine seasonal variations in the LDI. This transect has been previously studied for Saharan dust deposition in terms of grain sizes (van der Does et al., 2016), as the tropical North Atlantic receives approximately one-third of the wind-blown Saharan dust (e.g., Duce et al., 1991; Stuut et al., 2005), which might potentially act as fertilizer because of the high iron levels (e.g., Martin and Fitzwater, 1988; Korte et al., 2017; Guerreiro et al., 2017; Goudie and Middleton, 2001, and references therein). Furthermore, Korte et al. (2017) assessed mass fluxes and mineralogical composition, Guerreiro et al. (2017) measured coccolith fluxes for two of the time series, and Schreuder et al. (2018a, b) measured long-chain *n*-alkanes, long-chain *n*-alkanols and fatty acids, and levoglucosan for the same sediment trap samples and surface sediments as analyzed in this study.

At site M1 (12.00° N, 23.00° W), the sediment trap, referred to as M1U, was moored at a water depth of 1150 m (Fig. 1). This mooring is located in the proximity of the Guinea Dome; therefore, it might potentially be influenced by seasonal upwelling. At station M2 (13.81° N, 37.82° W), two sediment traps were recovered, i.e., an "upper" (M2U) trap at a water depth of 1235 m, and a "lower" (M2L) trap at a depth of 3490 m. Lastly, at mooring station M4 (12.06° N, 49.19° W), an upper and lower trap series were also recov-

ered and analyzed (M4U and M4L), at depths of 1130 and 3370 m, respectively. This mooring site may be seasonally affected by Amazon River discharge (van der Does et al., 2016; Korte et al., 2017; Guerreiro et al., 2017; Schreuder et al., 2018a). All sediment traps were equipped with 24 sampling cups, which sampled synchronously over 16-day intervals from October 2012 to November 2013, using HgCl$_2$ as a biocide and borax as a pH buffer to prevent in situ decomposition of the collected material.

2.1.2 Mozambique Channel

The Mozambique Channel is located between Madagascar and Mozambique and is part of the Agulhas Current system hugging the coast of South Africa (Lutjeharms, 2006). The Agulhas Current system is an important conveyor in the transport of warm and salty waters from the Indian Ocean to the Atlantic Ocean (Gordon, 1986; Weijer et al., 1999; Peeters et al., 2004). The northern part of the channel is also influenced by the east African monsoon winds (Biastoch and Krauss, 1999; Sætre and da Silva, 1984; Malauene et al., 2014). Between September and March, these winds blow from the northeast, parallel to the Mozambique coastline, favoring coastal upwelling. Additionally, the Mozambique Channel is largely influenced by fast-rotating, mesoscale eddies that migrate southward towards the Agulhas region. Using satellite altimetry, Schouten et al. (2003) observed four to six eddies on average, ca. 300 km in diameter, propagating yearly from the central Mozambique Channel (15° S) toward the Agulhas area (35° S) between 1995 and 2000. Seasonal upwelling occurs off northern Mozambique (between ca. 15 and 18° S) (Nehring et al., 1984; Malauene et al., 2014), from August to March with a dominant period of about 2 months although periods of 1–4 weeks have also been observed (Malauene et al., 2014).

The sediment trap was moored at 16.8° S and 40.8° E, at a water depth of 2250 m (Fig. 1; Fallet et al., 2010, 2011) and was the same type as that used for the North Atlantic transect. We analyzed the LCD proxies for two respective time intervals: the first interval covered ca. 3.5 years, from November 2003 to September 2007, with a sampling interval of 21 days. The second interval covered another year, between February 2008 and February 2009, with a sampling interval of 17 days. Previously, Fallet et al. (2011) published foraminiferal, U$_{37}^{K'}$ and TEX$_{86}$ records for the first time interval, and the organic carbon content for the follow-up time series. For further details on the deployments and sample treatments, we refer to Fallet et al. (2011, 2012). The two surface sediments are located across the narrowest transect between Mozambique and Madagascar, and were analyzed for U$_{37}^{K'}$ and TEX$_{86}$ by Fallet et al. (2012) and for LCDs by Lattaud et al. (2017b).

2.1.3 Cariaco Basin

The Cariaco Basin is one of the largest marine anoxic basins (Richards, 1975), located on the continental shelf of Venezuela. The basin is characterized by permanent stratification and is strongly influenced by the migration of the intertropical convergence zone (ITCZ). During late autumn and winter, the ITCZ migrates to the south which results in decreased precipitation and trade wind intensification that in turn induces upwelling and surface water cooling. This seasonal upwelling is a major source of nutrients that leads to strong phytoplankton growth along the Venezuelan coast (e.g., Müller-Karger et al., 2001; Thunell et al., 2007). Between August and October, the ITCZ moves northward again, resulting in a rainy season and diminishing the trade winds which inhibits upwelling. During this wet season the contribution of terrestrially derived nutrients is higher. Due to the prevalent anoxic conditions in the basin, there is no bioturbation; this has resulted in the accumulation of laminated sediments that provide excellent annually to decadally resolved climate records (e.g., Peterson et al., 1991; Hughen et al., 1996, 1998). Moreover, in November 1995, a time series experiment started to facilitate research on the link between biogeochemistry and the downward flux of particulate material under anoxic and upwelling conditions (Thunell et al., 2000). This project (CARIACO; http://imars.marine.usf.edu/cariaco, last access: November 2018) involved hydrographic cruises (monthly), water column chemistry measurements and sediment trap sampling (every 14 days). One mooring containing four automated sediment traps (Honjo and Doherty, 1988) was deployed at 10.50° N and 64.67° W, at a bottom depth of around 1400 m. These traps were moored at a depth of 275 m, just above the oxic/anoxic interface (Trap A), at 455 m (Trap B), at 930 m (Trap C) and at 1255 m (Trap D). All traps contained a 13-cup carousel which collected sinking particles over 2 weeks, and were serviced every 6 months. For further details on trap deployment and recovery, and sample collection, storage and processing we refer the reader to Thunell et al. (2000) and Goñi et al. (2004). In addition to the sediment trap sampling, the primary productivity of the surface waters was measured every month using ^{14}C incubations (Müller-Karger et al., 2001, 2004). For this study, we investigated two periods, i.e., May 1999–May 2000 and July 2002–July 2003 for traps A and B. These years include upwelling and non-upwelling periods, as well as a disastrous flooding event in December 1999 (Turich et al., 2013). Turich et al. (2013) identified the upwelling periods, linked to the migration of the ITCZ, as indicated by decreasing SST in the CTD (temperature at −1 m water depth) and satellite-based measurements (indicated by grey boxes in Figs. 8 and 10), and shoaling of the average depths of primary production and increased primary production. Moreover, Turich et al. (2013) evaluated the U$_{37}^{K'}$ and TEX$_{86}$ proxies for the same two time series for which we analyzed the LCD proxies.

2.2 Instrumental data

Satellite SST, precipitation and wind speed time series of the M1, M2 and M4 moorings in the Atlantic derive from Guerreiro et al. (2017, 2019), who retrieved these data from the Ocean Biology Processing Group (OBPG, 2014; Frouin et al., 2003), the Goddard Earth Sciences Data and Information Services Center (2016) (Huffman et al., 2007; Xie and Arkin, 1997) and the NASA Aquarius project (2015a, b) (Lee et al., 2012) (see Supplement of Guerreiro et al., 2017 for detailed references). The SST and chlorophyll a time series data for the Mozambique Channel were adapted from Fallet et al. (2011), who retrieved these data from the Giovanni database (for details see Fallet et al., 2011). Surface sediment proxy temperatures were compared to annual mean SST estimates derived from the World Ocean Atlas (2013) (decadal averages from 1955 to 2012; Locarnini et al., 2013). Sea surface temperature data for the Cariaco Basin were adopted from Turich et al. (2013) and combined with additional CTD temperatures from the CARIACO time series database for depths of 2, 5, 10, 15 and 20 m (http://www.imars.usf.edu/CAR/index.html, last access: November 2018; CARIACO time series composite CTD profiles; lead principal investigator: Frank Müller-Karger).

2.3 Lipid extraction

2.3.1 Tropical North Atlantic

The 120 sediment trap samples were sieved through a 1 mm mesh wet-split into five aliquots (van der Does et al., 2016), of which one was washed with Milli-Q water, freeze-dried and homogenized for chemical analysis (Korte et al., 2017). For organic geochemistry, sub-aliquots (by weight) were extracted as described by Schreuder et al. (2018a). Briefly, ca. 100 mg dry weight of sediment trap residue and between 1.5 and 10 g dry weight of surface sediment were extracted by ultrasonication using a mixture of dichloromethane : methanol (DCM/MeOH) (2 : 1; v/v), and were dried over a Na_2SO_4 column. For quantification of LCDs, LCAs and GDGTs, we added the following internal standards to the total lipid extracts (TLEs): 2.04 µg C_{22} 7,16-diol (Rodrigo-Gamiz et al., 2015), 1.50 µg 10-nonadecanone ($C_{19:0}$ ketone) and 0.1 µg C_{46} GDGT (Huguet et al., 2006), respectively. Subsequently, the TLEs were separated into apolar (containing n-alkanes), ketone (containing LCAs) and polar (containing LCDs and GDGTs) fractions over an activated (2 h at 150 °C) Al_2O_3 column by eluting with hexane/DCM (9 : 1; v/v), hexane/DCM (1 : 1; v/v) and DCM/MeOH (1 : 1; v/v), respectively. The apolar fractions were analyzed by Schreuder et al. (2018a) for n-alkanes. Polar fractions were split for GDGT (25 %) and LCD (75 %) analysis. The LCD fraction was silylated by the addition of BSTFA (N,O-bis(trimethylsilyl)trifluoroacetamide) and pyridine, and were heated at 60 °C for 20 min, after which

ethyl acetate was added prior to analysis. The ketone fraction was also dissolved in ethyl acetate, and analyzed by GC (gas chromatography) and GC/MS (gas chromatography mass spectrometry). The GDGT fraction was dissolved in hexane/isopropanol (99 : 1, v/v), filtered through a 0.45 µm polytetrafluoroethylene (PTFE) filter and analyzed by HPLC-MS (high-performance liquid chromatography – mass spectrometry).

2.3.2 Mozambique Channel

Aliquots of the sediment trap samples from the Mozambique Channel were previously extracted and analyzed by Fallet et al. (2011) and Fallet et al. (2012), respectively. The sediment trap material was extracted by ultrasonication using a mixture of DCM/MeOH (2 : 1; v/v), dried over Na_2SO_4, and separated into apolar, ketone and polar fractions via alumina pipette column chromatography, by eluting with hexane/DCM (9 : 1; v/v), hexane/DCM (1 : 1; v/v) and DCM/MeOH (1 : 1; v/v), respectively. These existing polar fractions of the sediment trap material were silylated (as described above), dissolved in ethyl acetate and reanalyzed for LCDs by GC-MS. As no record was kept of the division of the extracts and polar fractions into aliquots, we report the results in relative abundance rather than concentrations and fluxes of diols.

2.3.3 Cariaco Basin

Sediment trap material was extracted as described by Turich et al. (2013). Briefly, 1/16 aliquots of the trap samples were extracted by means of Bligh–Dyer extraction with sonication using a phosphate buffer and a trichloroacetic acid (TCA) buffer. The extracts were then separated by adding 5 % NaCl in solvent-extracted distilled deionized water, the organic phase was collected, and the aqueous phase was extracted twice more. The extracts were pooled and dried over Na_2SO_4 and separated by means of Al_2O_3 column chromatography, eluting with hexane/DCM (9 : 1; v/v), DCM/MeOH (1 : 1; v/v) and MeOH. For this study, the DCM/MeOH (1 : 1; v/v) fraction was silylated (as described above), dissolved in ethyl acetate, and analyzed for LCDs using GC-MS. Similar to the Mozambique Channel samples, no record was kept of the division of extracts and polar fractions into aliquots; thus, we report the results in relative abundance.

2.4 Instrumental analysis

2.4.1 GDGTs

The GDGT fractions of the surface sediments and sediment traps SPM samples of the tropical North Atlantic were analyzed for GDGTs using ultra-high-performance liquid chromatography mass spectrometry (UHPLC-MS). We used an Agilent 1260 HPLC, which was equipped with an automatic injector, interfaced with a 6130 Agilent MSD and HP Chem-

Station software according to Hopmans et al. (2016). Compound separation was achieved by two silica BEH HILIC columns in tandem (150 mm × 2.1 mm; 1.7 µm; Waters ACQUITY) in normal phase, at 25 °C. GDGTs were eluted isocratically for 25 min with 82 % A and 18 % B, followed by a linear gradient to 35 % B in 25 min and finally a linear gradient to 100 % B in the last 30 min. "A" denotes hexane; "B" denotes hexane/isopropanol (9 : 1; v/v). The flow rate was constant at 0.2 mL min^{-1}, and the injection volume was 10 µL. The APCI-MS (atmospheric pressure chemical ionization – mass spectrometry) conditions are described by Hopmans et al. (2016). Detection and quantification of GDGTs was achieved in selected ion monitoring mode (SIM) mode of the protonated molecules ([M + H]$^+$) of the GDGTs. We used a mixture of crenarchaeol and C$_{46}$ GDGT (internal standard) to assess the relative response factor, which was used for quantification of the GDGTs in the samples (cf. Huguet et al., 2006).

Sea surface temperatures were calculated by means of the TEX$_{86}^{H}$ as defined by Kim et al. (2010), which is a logarithmic function of the original TEX$_{86}$ index (Schouten et al., 2002):

$$TEX_{86}^{H} = \log \frac{[GDGT-2] + [GDGT-3] + [Cren']}{[GDGT-1] + [GDGT-2] + [GDGT-3] + [Cren']}, \quad (1)$$

where the numbers indicate the number of cyclopentane moieties of the isoprenoid GDGTs, and Cren' reflects an isomer of crenarchaeol, i.e., containing a cyclopentane moiety with a *cis* stereochemistry (Sinninghe Damsté et al., 2018). The TEX$_{86}^{H}$ values were translated to SSTs using the core-top calibration of Kim et al. (2010):

$$SST = 68.4 \times TEX_{86}^{H} + 38.6 \quad (2)$$

The branched isoprenoid tetraether (BIT) index is a proxy for the relative contribution of terrestrially derived organic carbon (Hopmans et al., 2004). We calculated the modified version as reported by de Jonge et al. (2014, 2015) which is based on the original index as proposed by Hopmans et al. (2004), but includes the 6-methyl brGDGTs:

$$BIT = \frac{[brGDGT\ Ia] + [brGDGT\ IIa+IIa'] + [brGDGT\ IIIa+IIIa']}{[brGDGT\ Ia] + [brGDGT\ IIa+IIa'] + [brGDGT\ IIIa+IIIa'] + [Cren]}, \quad (3)$$

where the numbers reflect different branched GDGTs (see Hopmans et al., 2004) and Cren reflects crenarchaeol. The branched GDGTs were always around the detection limit in the Atlantic samples, implying a BIT index of around zero and thus minimal influence of soil organic carbon (Hopmans et al., 2004); therefore, the BIT index is not discussed any further.

2.4.2 LCAs

The ketone fractions of the surface sediments and sediment traps samples of the tropical North Atlantic were analyzed for LCAs on an Agilent 6890N gas chromatograph (GC) with flame ionization detection (FID) after being dissolved in ethyl acetate. The GC was equipped with a fused silica column with a length of 50 m, a diameter of 0.32 mm and a coating of CP Sil-5 (film thickness = 0.12 µm). Helium was used as the carrier gas, and the flow mode was a constant pressure of 100 kPa. The ketone fractions were injected on-column at a starting temperature of 70 °C, which was increased by 20 °C min^{-1} to 200 °C followed by 3 °C min^{-1} until the final temperature of 320 °C was reached. This end temperature was held for 25 min.

The U$_{37}^{K'}$ index was calculated according to Prahl and Wakeham (1987):

$$U_{37}^{K'} = \frac{[C_{37:2}]}{[C_{37:2}] + [C_{37:3}]} \quad (4)$$

The U$_{37}^{K'}$ values were translated to SST following the calibration of Müller et al. (1998):

$$SST = \frac{U_{37}^{K'} - 0.044}{0.033} \quad (5)$$

We also applied the recently proposed BAYSPLINE Bayesian calibration of Tierney and Tingley (2018). They and others have shown that the U$_{37}^{K'}$ estimates substantially attenuate above temperatures of 24 °C (e.g., Conte et al., 2001; Goñi et al., 2001; Sicre et al., 2002). The Bayesian calibration moves the upper limit of the U$_{37}^{K'}$ calibration from approximately 28 to 29.6 °C at unity. As our traps are located in tropical regions with SSTs > 24 °C, we applied this calibration as well.

2.4.3 LCDs

The silylated polar fractions were injected on-column on an Agilent 7890B GC coupled to an Agilent 5977A MS. The starting temperature was 70 °C, and was increased to 130 °C by 20 °C min^{-1}, followed by a linear gradient of 4 °C min^{-1} to an end temperature of 320 °C, which was held for 25 min. A total of 1 µL was injected, and separation was achieved on a fused silica column (25 × 0.32 mm) coated with CP Sil-5 (film thickness 0.12 µm). Helium was used as the carrier gas with a constant flow of 2 mL min^{-1}. The MS operated with an ionization energy of 70 eV. Identification of LCDs was carried out in full scan mode, scanning between m/z 50 and 850, based on characteristic fragmentation patterns (Volkman et al., 1992; Versteegh et al., 1997). Proxy calculations and LCD quantifications were performed via analysis (in SIM mode) of the characteristic fragments (m/z 299, 313, 327 and 341; Rampen et al., 2012; m/z 187 for internal diol standard). For quantification of LCDs in the sediment traps and seafloor sediments of the tropical Atlantic, the peak areas of the LCDs were corrected for the average relative contribution of the selected SIM fragments to the total ion counts, i.e., 16 % for the saturated LCDs, 9 % for unsaturated LCDs and 25 % for the C$_{22}$ 7,16-diol internal standard.

Sea surface temperatures were calculated using the LDI, according to Rampen et al. (2012):

$$LDI = \frac{[C_{30}\ 1,15\text{-diol}]}{[C_{28}\ 1,13\text{-diol}] + [C_{30}\ 1,13\text{-diol}] + [C_{30}\ 1,15\text{-diol}]} \quad (6)$$

These LDI values were converted into SSTs using the following equation (Rampen et al., 2012):

$$SST = \frac{LDI - 0.095}{0.033} \quad (7)$$

Upwelling conditions were reconstructed using the diol index as proposed by Rampen et al. (2008):

$$Diol\ index = \frac{[C_{28}\ 1,14\text{-diol}] + [C_{30}\ 1,14\text{-diol}]}{[C_{28}\ 1,14\text{-diol}] + [C_{30}\ 1,14\text{-diol}] + [C_{30}\ 1,15\text{-diol}]} \quad (8)$$

In 2010, Willmott et al. introduced an alternative diol index, which is defined as the ratio of 1,14-diols over 1,13-diols. As the index of Rampen et al. (2008) includes the C_{30} 1,15-diol, it can be affected by temperature variation; therefore, we would normally prefer to use the index of Willmott et al. (2010). However, we often did not detect the C_{28} 1,13-diol, or it co-eluted with cholest-5-en-7-one-3β-ol, compromising the calculation of the diol index of Willmott et al. (2010). Moreover, the temperature variations in all three sediment traps are minimal as recorded by the LDI. Accordingly, we chose to apply the diol index according to Rampen et al. (2008).

Potential fluvial input of organic carbon was determined by the fractional abundance of the C_{32} 1,15-diol (de Bar et al., 2016; Lattaud et al., 2017a):

$$FC_{32}\ 1,15\text{-diol} = \frac{[C_{32}\ 1,15\text{-diol}]}{[C_{28}\ 1,13\text{-diol}] + [C_{30}\ 1,13\text{-diol}] + [C_{30}\ 1,15\text{-diol}] + [C_{32}\ 1,15\text{-diol}]} \quad (9)$$

The fractional abundance of the C_{32} 1,15-diol was always lower than 0.23, suggesting low input of river-derived organic carbon (Lattaud et al., 2017a).

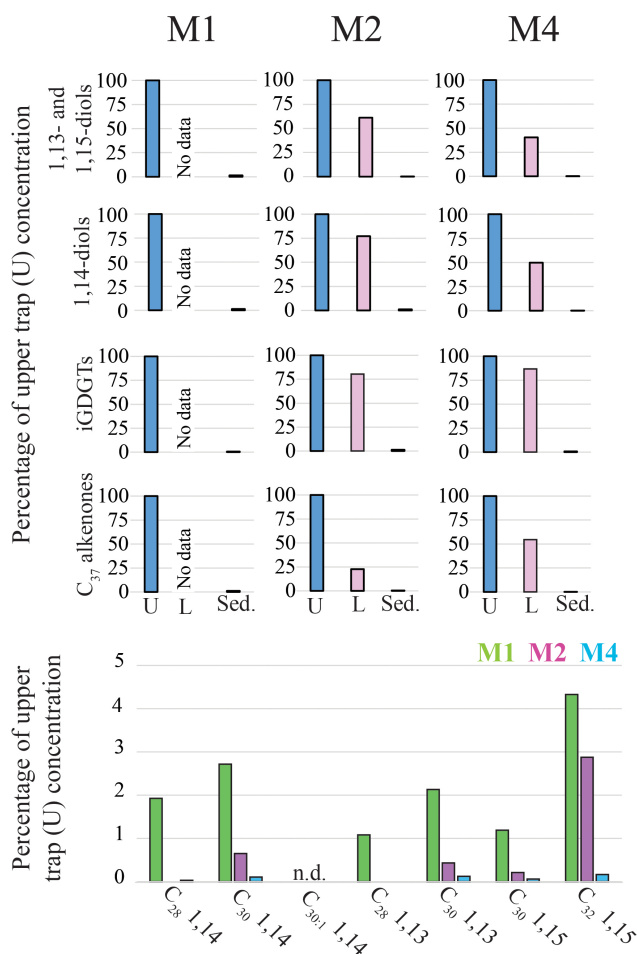## 3 Results

3.1 Tropical North Atlantic

We analyzed sediment trap samples from a longitudinal transect ($\sim 12°$ N) in the tropical North Atlantic (two upper traps at a depth of ca. 1200 m, and three lower traps at ca. 3500 m; Fig. 1), covering November 2012–November 2013, as well as seven underlying surface sediments, for LCDs, LCAs and GDGTs. Below we present the results for these lipid biomarkers and associated proxies.

3.1.1 LCDs

The LCDs detected in the sediment trap samples and surface sediments from the tropical North Atlantic (Fig. 2) are the

Figure 2. Relative concentrations of biomarker lipids for the M1, M2 and M4 mooring sites in the tropical North Atlantic. Upper panels show the percentages of lipid biomarkers in the lower traps ("L"; 3500 m) and the surface sediments ("Sed.") relative to the annual flux-weighted concentrations in the upper traps ("U"; 1200 m; set at 100 %). The lower panel shows the preservation of the individual LCDs (sediments versus upper trap flux-weighted concentration) for the three sediment trap sites. For M1 and M2 the sedimentary LCD concentrations were based on the average of the two nearby underlying surface sediments (Fig. 1). When no bar is shown the LCD was not detected in the surface sediments.

C_{28}, C_{30} and $C_{30:1}$ 1,14- (not in surface sediments), C_{28} and C_{30} 1,13-, and the C_{30} 1,15-, and C_{32} 1,15-diols. We detected the C_{28} 1,14-diol and C_{29}-OH fatty acid in the traps from M1 and M4, in a few samples of the M2 traps and in all surface sediments. For most samples from M2U and M2L, the C_{28} 1,14-diol was often part of a high background signal, making identification and quantification problematic. In these cases, 1,14-diol fluxes and the diol index were solely based on the (saturated and monounsaturated) C_{30} 1,14-diol.

The average [1,13+1,15]-diol flux is 2.6 (± 1.0) μg m^{-2} d^{-1} at M1U, 1.4 (± 1.2) and 1.2 (± 1.1) μg m^{-2} d^{-1} for M2U and M2L, respectively,

and 7.0 ($\pm$7.8) and 2.2 ($\pm$3.3) µg m^{-2} d^{-1} for M4U and M4L, respectively (Fig. 3). The [1,13+1,15]-diol and 1,14-diol concentrations in the underlying sediments vary between 0.05 and 0.50 µg g^{-1} and between 3 ng g^{-1} and 0.06 µg g^{-1}, respectively. The 1,14-diol flux for M1U averages 0.5 ($\pm$0.8) µg m^{-2} d^{-1} with a pronounced maximum of 3.5 µg m^{-2} d^{-1} in late April (Fig. 5a), irrespective of the total mass flux. The average 1,14-diol flux at M2 is much lower and is similar for the upper and lower traps, being around 0.01–0.02 ($\pm$0.01) µg m^{-2} d^{-1}. At M4, the average 1,14-diol fluxes are 0.3 ($\pm$0.5) and 0.1 ($\pm$0.2) µg m^{-2} d^{-1} for the upper and lower trap, respectively. There are two evident maxima in the [1,13+1,15]-diols and 1,14-diol fluxes in late April and during October/November, concomitant with maxima in the total mass flux (Fig. 3d, e). However, in the lower trap this flux maximum is distributed over two successive trap cups, corresponding to late April/early May (Fig. 3e, j).

The LDI ranged between 0.95 and 0.99 in all traps, corresponding to temperatures of 26.0 to 27.3 °C with no particular trends (Fig. 4). For most M2 and M4 samples the C$_{28}$ 1,13-diol was below the quantification limit; hence, LDI was always around unity, corresponding to 26.9 to 27.3 °C (Fig. 4), whereas in other samples the C$_{28}$ 1,13-diol co-eluted with cholest-5-en-7-one-3β-ol, prohibiting the calculation of the LDI and the diol index (Figs. 4, 5). The flux-weighted annual average LDI-derived SSTs were 26.6 °C for M1U, and 27.1 °C for M2U, M2L, M4U and M4L. The underlying sediment was very similar, with LDI values of between 0.95 and 0.98 corresponding to 26.0 and 26.9 °C (Fig. 6). The diol index varied from 0.03 to 0.30 in M1U, showing a pronounced maximum during spring (Fig. 5a). The diol index at M2 ranged between 0.01 and 0.03 without an evident pattern, whereas the diol index at M4 ranged from 0.01 to 0.10 and showed the same pattern in the lower and upper trap, with the highest values during spring (ca. 0.1), followed by a gradual decrease during summer (Fig. 5e, f).

3.1.2 LCAs

We detected C$_{37}$, C$_{38}$ and C$_{39}$ long-chain alkenones in the sediment trap and surface sediments. The C$_{37:3}$ alkenone was generally around the limit of quantification for the M2L and M4L traps, and below the limit of quantification for four out of the seven surface sediment samples, whereas the C$_{37:2}$ alkenone was always sufficiently abundant. The annual mean fluxes of the C$_{37}$ LCAs were 4.3 ($\pm$3.5) µg m^{-2} d^{-1} for M1U, 1.2 ($\pm$0.9) µg m^{-2} d^{-1} and 0.4 ($\pm$0.2) µg m^{-2} d^{-1} for M2U and M2L, respectively, and 2.9 ($\pm$5.1) µg m^{-2} d^{-1} and 1.2 ($\pm$2.0) µg m^{-2} d^{-1} for M4U and M4L, respectively. The concentrations of the C$_{37}$ LCAs in the underlying surface sediments ranged between 0.02 and 0.41 µg g^{-1}. At M4, the two total mass flux peaks at the end of April and during October/November were also clearly pronounced in the C$_{37}$ alkenone fluxes (Figs. 3d, e, 5g), as well as the in-

creased signal in the cup reflecting the beginning of May, which followed the cup which recorded the peak in total mass flux at the end of April. The U$_{37}^{K'}$ varied from 0.87 to 0.93, corresponding to 25.1 to 27.0 °C (Fig. 6b) for three out of seven surface sediments in which the C$_{37:3}$ was above the quantification limit. The flux-weighted average SSTs were 26.1 °C for M1U, 25.7 and 26.4 °C for M2U and M2L, respectively, and 28.2 and 27.5 °C for M4U and M4L, respectively (Fig. 6). SST variations per sediment trap were generally within a 2–3 °C range (Fig. 4) with no apparent trends.
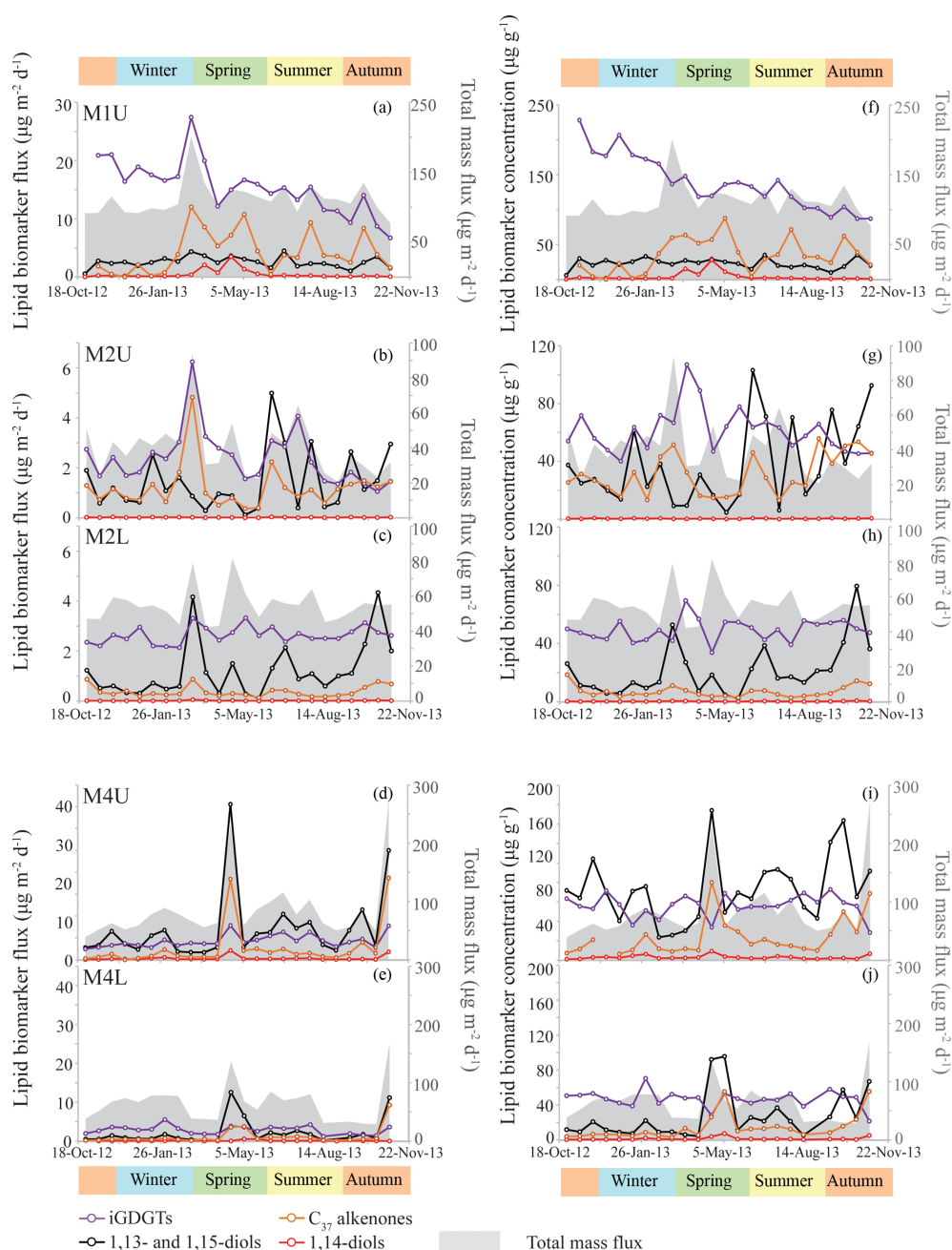
3.1.3 GDGTs

The main GDGTs detected were the isoprenoidal GDGT-0, -1, -2, -3, crenarchaeol and the isomer of crenarchaeol. Branched GDGTs were typically around or below quantification limit. The average iGDGT flux in M1U was 15.5 ($\pm$4.6) µg m^{-2} d^{-1}, 2.4 ($\pm$1.1) and 2.6 ($\pm$0.3) µg m^{-2} d^{-1} in M2U and M2L, respectively, and 4.3 ($\pm$1.5) and 2.9 ($\pm$1.2) µg m^{-2} d^{-1} in M4U and M4L, respectively (Fig. 3). The surface sediments exhibited iGDGT concentrations between 0.4 and 1.7 µg g^{-1}. Sediment TEX$_{86}^{H}$ values varied between 0.62 and 0.69, corresponding to 24.3 to 27.4 °C. The TEX$_{86}^{H}$ flux-weighted average SSTs were 25.2 °C for M1U, 27.3 and 26.6 °C for M2U and M2L, respectively, and 27.8 and 26.7 °C for M4U and M4L, respectively. SSTs typically varied within a range of 1–2 °C. At M2U, the TEX$_{86}^{H}$ temperatures decrease slightly (ca. 1–2 °C) between January and July (Fig. 4b).

3.2 Mozambique Channel

For two time series (November 2003–September 2007 and February 2008–February 2009), we analyzed LCDs collected in the sediment trap at a depth of 2250 m as well as nearby underlying surface sediments (Fig. 1). The main LCDs observed in the sediment traps and surface sediments were the C$_{28}$ 1,12-, 1,13- and 1,14-diols, the C$_{30}$ 1,13-, 1,14- and 1,15-diols, and the C$_{32}$ 1,15-diol. We also observed the C$_{30:1}$ 1,14 diol in some trap samples, and the C$_{29}$ 12-OH fatty acid in all trap and sediment samples. In 24 samples, the C$_{28}$ 1,13-diol co-eluted with cholest-5-en-7-one-3β-ol, and thereafter we did not calculate the LDI for these samples. The C$_{28}$ 1,14-diol was not affected by this cholest-5-en-7-one-3β-ol due to its much higher abundance compared with the C$_{28}$ 1,13-diol; therefore, the diol index was still calculated. The LDI varied between 0.94 and 0.99, i.e., close to unity, corresponding to 25.5 to 27.2 °C, without an evident trend (Fig. 7a). The diol index ranged between 0.11 and 0.69, showing substantial variation, although not with an evident trend (Fig. 7b). The average LDI-derived temperature of the two underlying surface sediments was 26.0 °C.
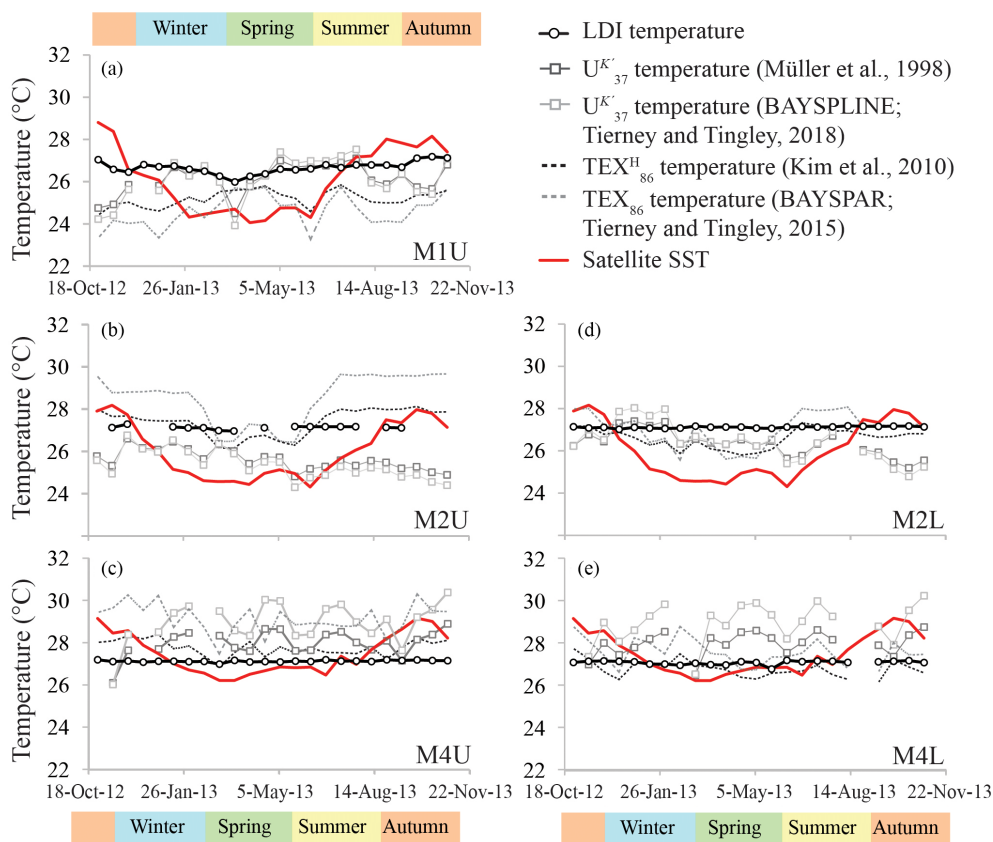
Figure 3. Lipid biomarker fluxes for the tropical North Atlantic sediment traps, i.e., M1, upper and lower M2, and upper and lower M4 in panels **(a)** to **(e)**. Lipid biomarker fluxes (iGDGTs in purple; C_{37} alkenones in orange; 1,13- and 1,15-diols in black; 1,14-diols in red) are indicated on the left y axis, and the total mass flux (grey stack; Korte et al., 2017) is shown on the right y axis. Lipid biomarker concentrations are plotted in panels **(f)** to **(j)**, with biomarker concentrations on the left y axis, and the total mass flux on the right y axis. Note that the y axes are different per sediment trap site, but identical for upper (U) and lower (L) traps.

3.3 Cariaco Basin

We analyzed LCDs for two time series (May 1999–May 2000 and July 2002–July 2003) from the upper (Trap A; 275 m) and the lower (Trap B; 455 m) trap in the Cariaco Basin. The main LCDs detected for both time series are the C_{28} 1,14-, C_{30} 1,14-, $C_{30:1}$ 1,14-, C_{28} 1,13-, C_{30} 1,15- and C_{32} 1,15-

diols, as well as the C_{29} 12-OH fatty acid. For some samples we did not compute the LDI, as the C_{28} 1,13-diol co-eluted with cholest-5-en-7-one-3β-ol. In a similar fashion to the Mozambique Channel, the C_{28} 1,14-diol was not affected by this co-elution due to its much higher abundance compared with the C_{28} 1,13-diol; therefore, the diol index was therefore

Figure 4. Temperature proxy records for the tropical North Atlantic. The panels show **(a)** the upper trap station M1, **(b)** the upper trap station M2 and **(d)** the lower trap M2, respectively, and **(c)** the upper trap station M4 and **(e)** lower trap station M4, respectively.

still calculated. The calculated LDI values ranged between 24.3 and 25.3 °C and 22.0 and 27.2 °C for Trap A and B of the 1999–2000 time series, respectively, with the lowest temperature during winter and the highest during summer. For the 2002–2003 time series, LDI temperatures for Trap A ranged between 23.3 and 26.2 °C and between 22.5 and 26.5 °C for Trap B.
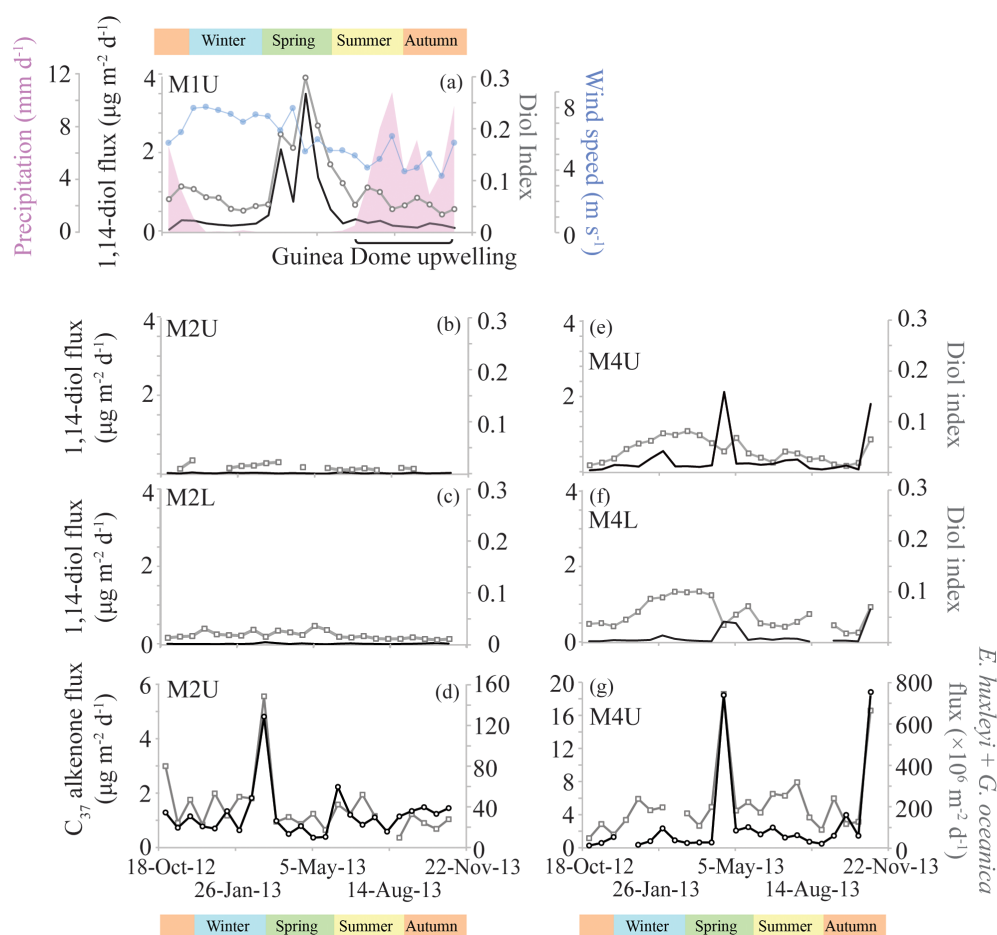
For the May 1999–May 2000 time series, the diol index varied between 0.05 and 0.97 for Trap A and between 0.05 and 0.91 for Trap B (Fig. 8) with similar trends, i.e., the lowest values of around 0.1–0.2 just before the upwelling period during November, rapidly increasing towards values between ca. 0.8 and 1 during the upwelling season (January and February). For the time series of July 2002–July 2003, the diol index showed similar trends, i.e., diol index values around 0.8–0.9 during July, which rapidly decrease towards summer values of around 0.2–0.3. Similar to the 1999–2000 time series, the lowest index values (ca. 0.2) are observed just before the upwelling period (during September), after which they increase towards values of around 0.8–0.9 between December and March at the start of the upwelling season. At the end of the upwelling season the diol index increases, followed by another maximum of around 0.6 during May.

4 Discussion

4.1 LCD sources and seasonality

The 1,14 diols can potentially be derived from two sources: *Proboscia* diatoms (Sinninghe Damsté et al., 2003; Rampen et al., 2007) or the dictyochophyte *Apedinella radians* (Rampen et al., 2011). The non-detection of the C_{32} 1,14-diol, which is a biomarker for *Apedinella radians* (Rampen et al., 2011), and the detection of the $C_{30:1}$ 1,14 diol and C_{29} 12-OH fatty acid, which are characteristic of *Proboscia* diatoms (Sinninghe Damsté et al., 2003), suggests that *Proboscia* diatoms are most likely the source of 1,14-diols in the tropical North Atlantic, the Mozambique Channel and the Cariaco Basin.

In the Cariaco Basin, the diol index shows a strong correlation (visually as correlation analysis was not possible due to differently spaced data in time) with primary production rates, suggesting that *Proboscia* productivity was synchronous with total productivity (Fig. 8), although for the 1999–2000 time series there is a disagreement during January/February. Primary productivity in the Cariaco Basin is largely related to seasonal upwelling which occurs between November and May when the ITCZ is at its southern posi-
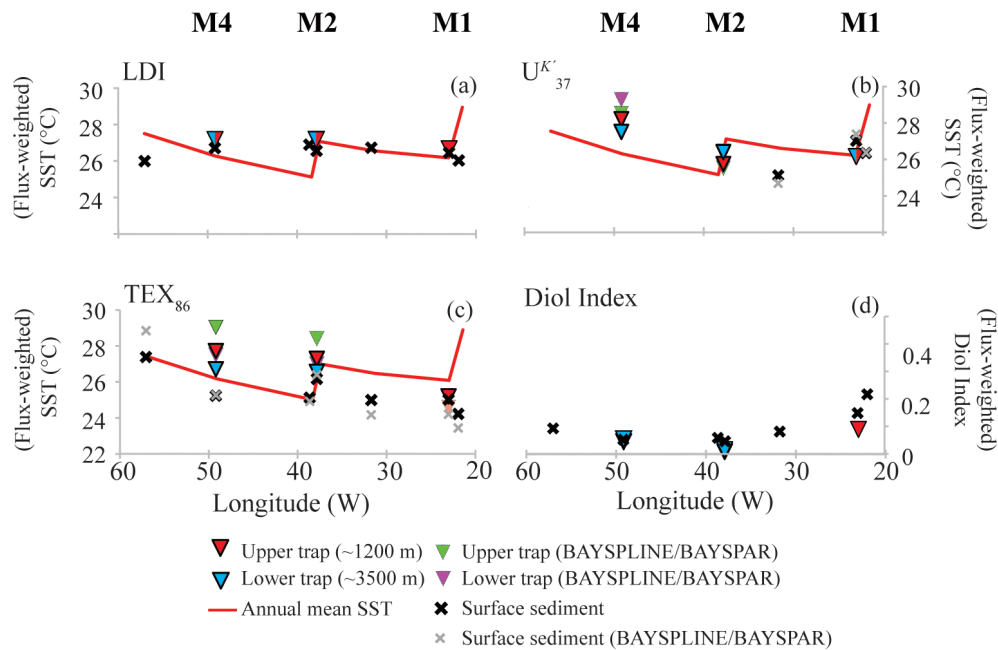
Figure 5. Phytoplankton productivity records for the tropical North Atlantic. Panels **(a)**–**(c)** and **(e)**–**(f)** show the 1,14-diol fluxes (left y axis; black) and the diol index (right y axis; grey) for the sediment traps. The y axes are the same for these panels. Wind speed and precipitation data were adapted from Guerreiro et al. (2019); for references regarding remote sensing parameters, see Guerreiro et al. (2017). Panels **(d)** and **(g)** show the C_{37} alkenone fluxes (left y axis; black) and combined fluxes of *Emiliania huxleyi* and *Gephyrocapsa oceanica* (from Guerreiro et al., 2017; right y axis; grey) for the upper traps of M2 and M4.
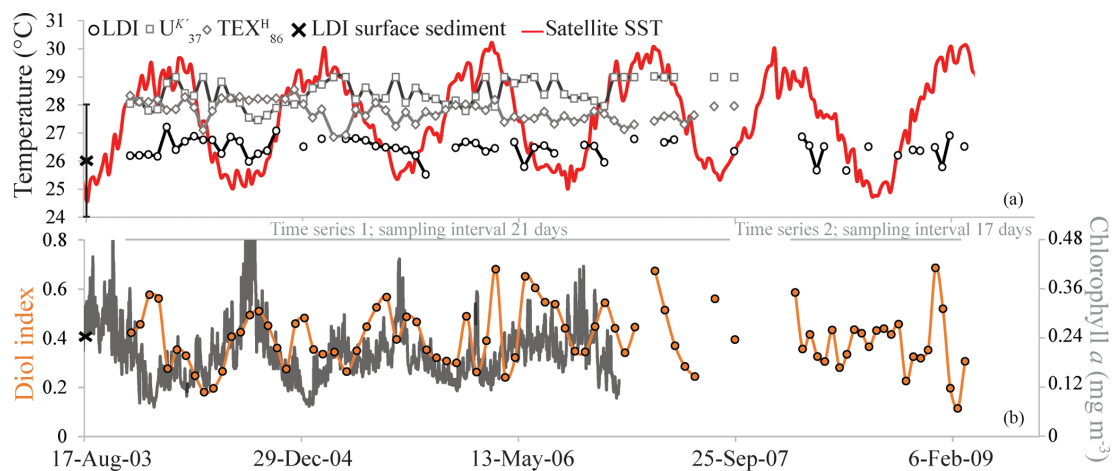
tion. Hence, the diol index seems to be an excellent indicator of upwelling intensity in the Cariaco Basin.

The index also shows considerable variation over time in the Mozambique Channel (Fig. 7b). Previous studies have shown that upwelling occurs in the Mozambique Channel between ca. 15 and 18° S (Nehring et al., 1984; Malauene et al., 2014), i.e., at the location of our sediment trap. Upwelling is reflected by cool water events and slightly enhanced chlorophyll *a* levels; Malauene et al. (2014) observed cool water events at ca. 2-month intervals although periods of 8 to 30 days were also noted. The two main potential forcing mechanisms for upwelling in the Mozambique Channel are the east African monsoon winds and the mesoscale eddies migrating through the channel. Fallet et al. (2011) showed that subsurface temperature, current velocity and the depth of surface-mixed layer all revealed a dominant periodicity of four to six cycles per year, which is the same frequency as that of the southward migration of mesoscale ed-

dies in the channel (Harlander et al., 2009; Ridderinkhof et al., 2010), implying that eddy passage strongly influences the water mass properties. Wavelet analysis of the diol index for the 2003–2007 period (Fig. S1 in the Supplement) revealed short periods, occurring around January of 2004, 2005 and 2006, of significant (above the 95 % confidence level) variability at about bimonthly frequencies (60-day period). Both the frequency (bimonthly) and the timing (boreal winter) of the observed time periods of the enhanced diol index variability are similar to those of the cool water events as observed by Malauene et al. (2014), associated with upwelling (Fig. 7b). The strongest variability of the diol index at about bimonthly frequencies occurred in the first half of 2006. During the same period, salinity time series showed the passage of several eddies that had a particularly strong effect on the upper layer hydrography (Ullgren et al., 2012). Malauene et al. (2014) showed that neither upwelling-favorable winds, nor passing eddies, can independently explain the observed
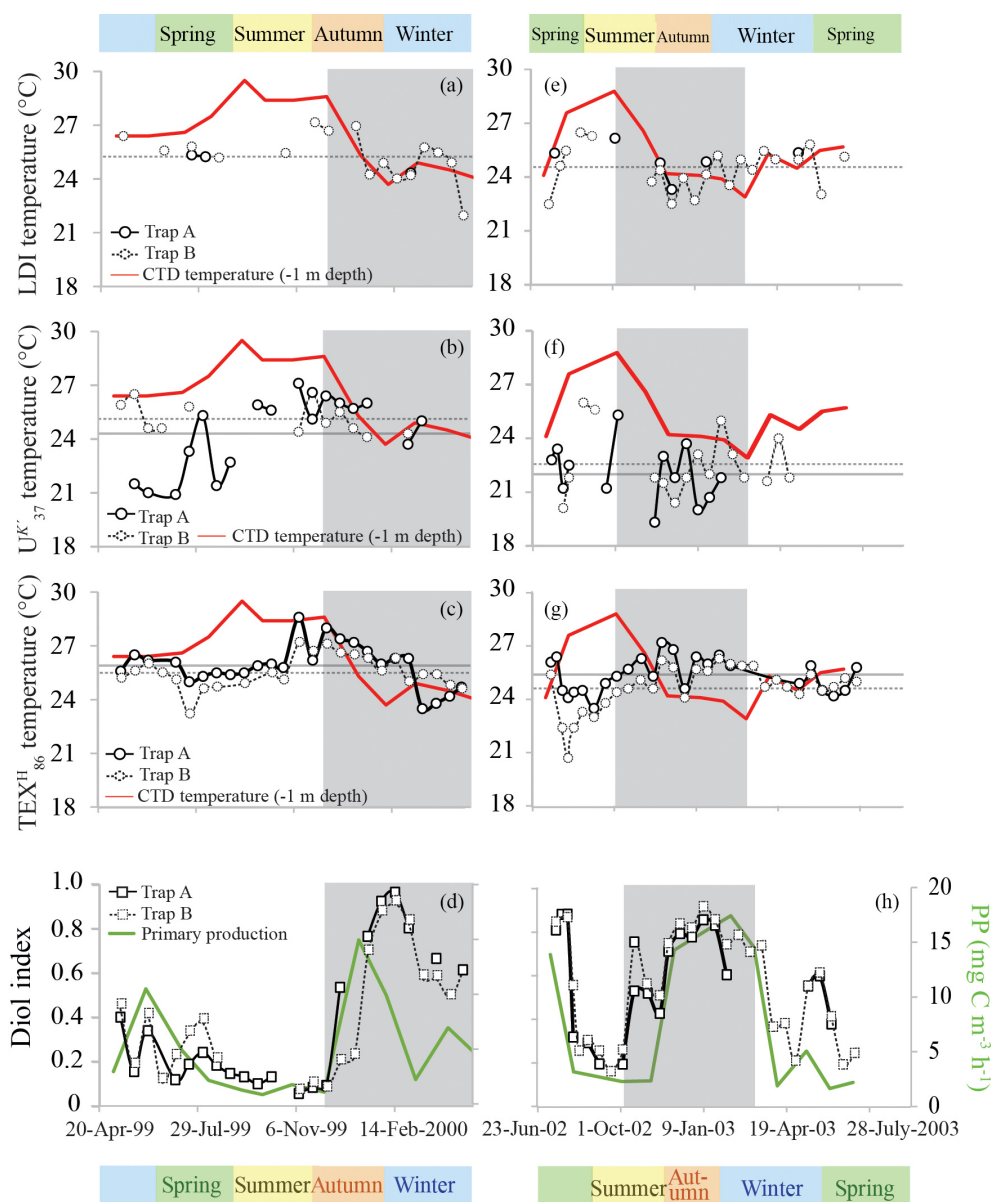
Figure 6. Flux-weighted average (annual) proxy results for the sediment traps compared with the underlying sediments (crosses) and annual mean SST (red line; specific for the coordinates of the surface sediments; World Ocean Atlas 2013 $1/4°$ grid resolution). Panels **(a)**, **(b)** and **(c)** show the LDI, $U_{37}^{K'}$ and TEX_{86} temperature results, respectively. Triangles reflect sediment trap results (red represents upper/$\sim$ 1200 m; blue represents lower/$\sim$ 3500 m), and crosses represent surface sediments. In the case of the $U_{37}^{K'}$ and TEX_{86}, the green and purple triangles and grey crosses reflect the temperatures calculated using the BAYSPLINE and BAYSPAR models (Tierney and Tingley, 2014, 2015, 2018), whereas the other temperatures were calculated using the Müller et al. (1998) and Kim et al. (2010; TEX_{86}^H) calibrations, respectively. Panel **(d)** shows the flux-weighted average diol index values for the sediment traps and the diol index estimates for the surface sediments.

Figure 7. The LDI-derived temperatures, in addition to the TEX_{86}^H and $U_{37}^{K'}$-derived temperatures and satellite SST (Fallet et al., 2011) **(a)** and the diol index **(b)** for the Mozambique Channel sediment trap. The black cross in panel **(a)** reflects the average LDI temperature of two underlying surface sediments, with the LDI calibration error. The chlorophyll a data are from Fallet et al. (2011).

upwelling along the northern Mozambique coast. The two processes may act together, and both strongly influence the upper water layer and the organisms living there, potentially including the LCD producers.

The least (seasonal) variation in the diol index is observed at M2 in the tropical North Atlantic (Fig. 5b, c), which is likely due to its central open ocean position, associated with relatively stable, oligotrophic conditions (Guerreiro et al., 2017). In contrast, M4 and M1 are closer to the South Amer-
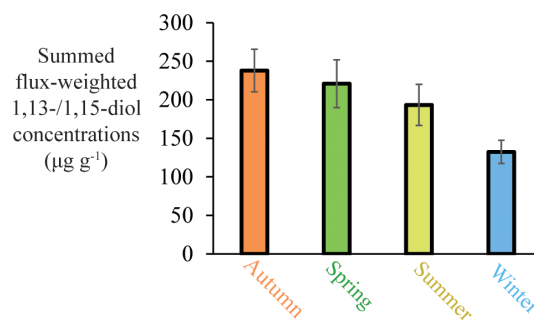
Figure 8. Seasonal proxy-derived temperature and upwelling/productivity records for the sediment traps in the Cariaco Basin. Panels **(a)**, **(b)** and **(c)** show the May 1999–May 2000 time series LDI-, $U_{37}^{K'}$- and TEX_{86}^{H}-derived temperature reconstructions for Trap A (depth of 275 m; solid symbols) and Trap B (depth of 455 m; dashed symbols), respectively. Panels **(e)**, **(f)** and **(g)** show the proxy data for the July 2002–July 2003 time series, with CTD-temperatures (1 m depth) in red. The $U_{37}^{K'}$, TEX_{86}^{H} and CTD temperatures are adopted from Turich et al. (2013). The horizontal lines reflect the average proxy-derived temperatures (Trap A is denoted using solid lines; Trap B is denoted using dashed lines). Panels **(d)** and **(h)** show the 1,14-diol based diol index (Rampen et al., 2008) for the 1999–2000 and 2002–2003 time series, respectively, for Trap A (depth of 275 m; solid symbols) and Trap B (depth of 455 m; dashed symbols). Primary productivity in mg C m^{-3} h^{-1} is plotted in green (data adopted from Turich et al., 2013). The shaded area reflects the period of upwelling.

ican and west African coast, respectively, and thus are potentially under the influence of Amazon river runoff and upwelling, respectively, and specific wind and ocean circulation regimes (see Sect. 2.1.1). However, at M4, the diol index is also low (max. 0.1), suggesting low *Proboscia* productivity (Fig. 5e, f). At M1, in contrast, we observe enhanced values for the diol index of up to ∼ 0.3 during spring (Fig. 5a).

Most likely, an upwelling signal at this location is associated with the seasonal upwelling of the Guinea Dome. This upwelling is generally most intense between July and October (Siedler et al., 1992), due to the northward movement of the ITCZ and the resulting intensified Ekman upwelling. Specifically, during this period, the trade winds are weaker, atmospheric pressure is lower and the regional wind stress

is favorable to upwelling of the North Equatorial Undercurrent (Voituriez, 1981). Indeed, a decrease in wind speed and increased precipitation from summer to autumn was observed (Fig. 5a) which confirms that during these seasons the ITCZ was indeed in a northern position, and that during 2013 the upwelling associated with the Guinea Dome was most favored between July and October. The timing of the diol index peak, i.e., between March and June, is consistent with previous sediment trap studies elsewhere which have shown that *Proboscia* diatoms and 1,14-diols are typically found during pre-upwelling or early upwelling periods (Koning et al., 2001; Smith, 2001; Sinninghe Damsté et al., 2003; Rampen et al., 2007). The surface sediment at 22° W just east of M1 also reveals the highest diol index (0.22), likely due to its closer vicinity to the Guinea Dome center. Several studies have reported *P. alata* diatoms offshore of northwest Africa (Lange et al., 1998; Treppke et al., 1996; Crosta et al., 2012; Romero et al., 1999), pointing to *P. alata* as a plausible source organism. The sedimentary annual diol indices compare well with the sediment trap indices (Fig. 6d), which is consistent with the results of Rampen et al. (2008). Our results clearly show that the diol index reflects different things in different regions. This is due to the ecology of *Proboscia* spp. where blooms occur during stratification, during early upwelling and post-bloom, and from high nutrients to low nutrients (see Rampen et al., 2014a; references in Table 1). Therefore, the type of conditions reflected by the diol index is specific for every region.

To assess variations in the seasonal production of 1,13- and 1,15-diols in the tropical Atlantic, for which we have the most complete data set, we calculated the flux-weighted 1,13- and 1,15-diol concentrations for the different traps, and summed these per season (Fig. 9). Highest production is observed in autumn, followed by spring and summer, with the lowest production during winter ($\sim 60\%$ compared with autumn). This is in agreement with Rampen et al. (2012) who observed, for an extensive set of surface sediments, the strongest correlation between LDI and SST for autumn, suggesting that production of the source organisms of the LDI mainly occurs during autumn. At M4, there are two evident peaks in the 1,13- and 1,15-diol fluxes at the end of April and October 2013. These maxima correlate with peaks in other lipid biomarker fluxes (i.e., 1,14-diols, C_{37} alkenones and iGDGTs), total mass flux, calcium carbonate ($CaCO_3$), OM (organic matter) and the residual mass flux which includes the deposition flux of Saharan dust (Korte et al., 2017). According to Guerreiro et al. (2017), the maximum in total mass flux at the end of April 2013 is likely caused by enhanced export production due to nutrient enrichment as a result of wind-forced vertical mixing. The peak at the end of October 2013, is likely associated with discharge from the Amazon River. Moreover, both peaks are concomitant with prominent dust flux maxima, suggesting that Saharan dust also acted as nutrient fertilizer (Korte et al., 2017; Guerreiro et al., 2017). Guirreirro et al. (2017) suggested that dur-

Figure 9. Seasonal summed flux-weighted average of 1,13-/1,15-diol concentrations in all sediment traps (station M1 upper trap, station M2 upper and lower trap, and station M4 upper and lower trap) of the tropical North Atlantic.

ing the October–November event the Amazon River may not only have acted as nutrient supplier, but also as buoyant surface density retainer of dust-derived nutrients in the surface waters, resulting in the development of algal blooms within just a few days, potentially explaining the peak 1,13- and 1,15-diol fluxes, as well as the peak fluxes of the other lipid biomarkers. However, they might also partially result from enhanced particle settling, caused by factors such as dust ballasting or faecal pellets of zooplankton (see Guerreiro et al., 2017, and references therein). This agrees with the results of Schreuder et al. (2018a) that show that the *n*-alkane flux also peaks concomitly with the peaks in total mass flux and biomarkers, whereas *n*-alkanes are terrestrially derived (predominantly transported by dust); therefore, increased deposition can not result from increased primary productivity in the surface waters.

The C_{37} alkenone flux at M4U also reveals these two distinct maxima at the end of April and October during 2013 (Fig. 5g). Interestingly, this flux, as well as the alkenone flux at M2U, is consistent with coccolith export fluxes of the species *Emiliania huxleyi* and *Gephyrocapsa oceanica* (Guerreiro et al., 2017). In fact, when we combine the coccolith fluxes of both species, we observe strong correlations with the C_{37} alkenone fluxes for both M2U and M4U (Fig. 5d and g, respectively; $r = 0.77$ and 0.92 for M2U and M4U, respectively; p-values < 0.001). This implies that these two species are the main LCA producers in the tropical North Atlantic, which agrees with previous findings (e.g., Marlowe et al., 1984; Brassell, 2014; Conte et al., 1994; Volkman et al., 1995).

4.2 Preservation of LCDs

The sediment trap data from the North Atlantic can be used to assess the relative preservation of LCDs, as well as other proxy lipid biomarkers, by comparing the flux-weighted concentration in the traps with the concentrations in the surface sediments. For all four biomarker groups, i.e., C_{37} alkenones, iGDGTs, 1,14-diols and 1,13- and 1,15-diols, we observe

that the flux-weighted concentrations are generally higher in the upper traps (ca. 1200 m) compared with the lower traps (ca. 3500 m; Fig. 2) by a factor of between 1.2 and 4.4, implying degradation during settling down the water column. The concentrations in the surface sediments are 2 to 3 orders of magnitude lower (i.e., between 0.1 %–1.5 % of upper trap signal), implying that degradation of lipids mainly takes place at the water–sediment surface rather than in the water column. A similar observation was made for levoglucosan in these sediment traps (Schreuder et al., 2018b). Both are functionalized polar lipids with alcohol groups and thus are chemically relatively similar when compared to species such as fatty acids (carboxyl group) or n-alkanes (no functional groups). These degradation rates are likely linked to the extent of the oxygen exposure time (Hartnett et al., 1998; Hedges et al., 1999) at the seafloor (Hartnett et al., 1998; Sinninghe Damsté et al., 2002), as during settling the lipids are exposed to oxygen for weeks, whereas for surface sediments this is typically decades to centuries. Our results compare well with several other sediment trap studies which showed that LCDs, LCAs and iGDGTs generally have a preservation factor of around 1 % (surface sediment versus trap) (e.g., Prahl et al., 2000; Wakeham et al., 2002; Rampen et al., 2007; Yamamoto et al., 2012).

We also identified the C_{30} and C_{32} 1,15-keto-ol in the Atlantic as well as in the Mozambique and Cariaco sediment traps and surface sediments. These lipids are structurally related to LCDs, occur ubiquitously in marine sediments (e.g., Versteegh et al., 1997, 2000; Bogus et al., 2012; Rampen et al., 2007; Sinninghe Damsté et al., 2003; Wakeham et al., 2002; Jiang et al., 1994) and were inferred to be oxidation products of LCDs (Ferreira et al., 2001; Bogus et al., 2012; Sinninghe Damsté et al., 2003). We did not detect 1,14-keto-ols, which supports the hypothesis of Ferreira et al. (2001) and Sinninghe Damsté et al. (2003) that the silica frustules of *Proboscia* diatoms sink relatively fast; thus, they are exposed to oxygen for a shorter period than the producers of 1,13- and 1,15-diols, and are therefore less affected by oxidation. Alternatively, the keto-ols are not oxidation products but are produced by unknown organisms in the water column. In fact, Méjanelle et al. (2003) observed trace amounts of C_{30} 1,13- and C_{32} 1,15-keto-ols in cultures of the marine eustigmatophyte *Nannochloropsis gaditana*. Thus, an alternative explanation for the non-detection of 1,14-keto-ols is that, in contrast to the 1,15-keto-ols, they were not produced in the water column.

For both the tropical Atlantic and the Cariaco Basin, we observe highly similar LDI values for the upper and the lower traps. In the Atlantic there is no statistical difference between the upper and lower traps that are 2200 m apart (two-tailed $p > 0.8$), but we have insufficient data for the Cariaco Basin for statistical comparison (Figs. 6a, 8a, e). This suggests that degradation in the water column does not affect the LDI proxy. This is in agreement with Reiche et al. (2018) who performed a short-term degradation experiment (< 1 year)
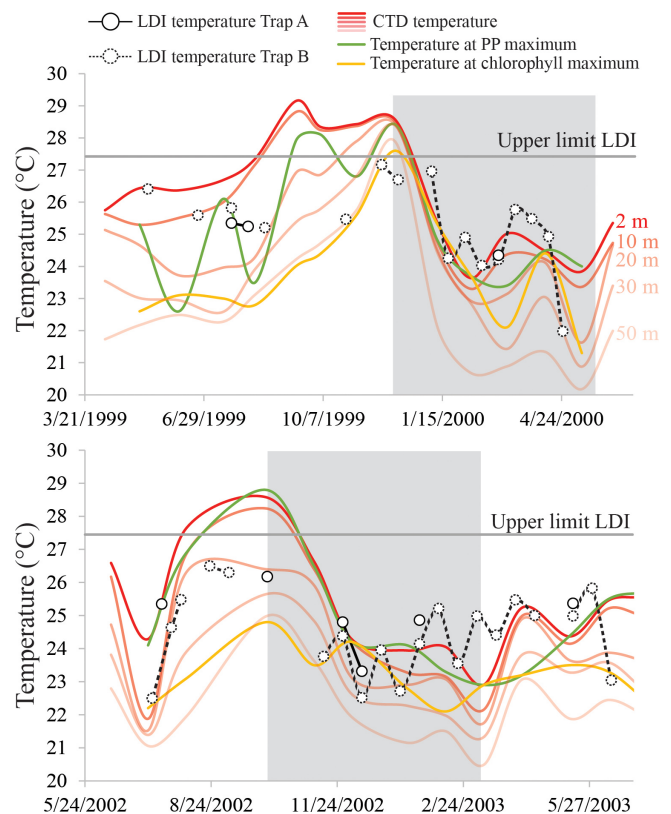
and found that the LDI index was not affected by oxic exposure on short timescales. However, the oxygen exposure time on the seafloor is much longer; Rodrigo-Gámiz et al. (2016) showed for sediments in the Arabian Sea (deposited under a range of bottom water oxygen conditions) that different LCDs had different degradation rates, which compromised the LDI ratio. For the three sites in the tropical North Atlantic, we calculated the flux-weighted average proxy values for every sediment trap and compare these with the underlying surface sediments (Fig. 6a–c). For all indices, i.e., diol index, LDI, $U^{K'}_{37}$ and TEX$_{86}$, we observe very good correspondence between the sediment trap and surface sediment values, implying minimal alteration of the proxies after settling and during burial. Similarly, for the Mozambique Channel, the mean diol index and LDI from the sediment trap (i.e., 0.41 and 0.97, respectively) are very similar to the surface sediment values (i.e., 0.42 and 0.95, respectively). In agreement with the consistent diol indices, we observe that all individual LCDs are also preserved relatively equally in the tropical Atlantic (1.2 %–4.3 % at station M1, 0.1 %–2.9 % at station M2 and 0.03 %–0.16 % at station M4). This contrasts with Rodrigo-Gámiz et al. (2016) who found that the 1,15-diols have the highest degradation rate, followed by the 1,14- and 1,13-diols. Only the C_{32} 1,15-diol seems relatively better preserved than the other LCDs at all three North Atlantic mooring sites (Fig. 2), suggesting that the C_{32} 1,15-diol is less impacted by degradation. The C_{32} 1,15-diol likely partially derives from the same source as the other 1,13- and 1,15-diols, but is also produced in fresh water systems (e.g., Versteegh et al., 1997, 2000; Rampen et al., 2014b; de Bar et al., 2016; Lattaud et al., 2017a, b). Hence, the different preservation characteristics might be the result of a different source for this LCD.

4.3 Relationship between LDI and SST

In the tropical Atlantic and the Mozambique Channel, the LDI-derived SSTs show minimal variability (< 2 °C), whereas in the Cariaco Basin we observe much larger changes that range from 22.0 to 27.2 °C (Fig. 8). Both time series in the Cariaco Basin show low temperatures between November and May, associated with the seasonal upwelling and surface water cooling, and significantly higher temperatures during the rainy summer. However, during the warmest periods, the LDI temperatures are generally lower than those measured at the surface by CTD, whereas during the colder phases, the LDI agrees well with the measurements. The LDI calibration reaches unity at 27.4 °C; therefore, is not possible to resolve the highest temperatures which are between ca. 28 and 30 °C. However, the LDI-derived temperatures are sometimes well below 27.4 °C where the CTD data suggest SSTs > 28 °C. Consequently, the LDI-based temperatures agree with CTD-based SSTs within calibration error for most of the record, but during summer when the SST is highest, they are offset outside the calibration error

($\Delta T \sim 2.5\,°C$). Interestingly, the $U_{37}^{K'}$- and TEX_{86}^H-derived temperature trends show the same phenomenon (Turich et al., 2013; Fig. 8), where the proxy temperatures are cooler than the measured temperatures during the warmer months. However, in contrast to the $U_{37}^{K'}$ and LDI, the TEX_{86}^H also overestimates the SST during the cold months. For $U_{37}^{K'}$, Turich et al. (2013) pointed out that a time lag between synthesis, export and deposition could potentially explain the difference between the proxy and CTD temperatures. However, previous analysis of plankton biomass, primary productivity, bio-optical properties and particulate organic carbon fluxes for the same time period (Müller-Karger et al., 2004), as well as the total mass and terrigenous fluxes assessed by Turich et al. (2013) showed the best correlation at zero-time lag on the basis of their 14-day sample interval. We compared our LDI temperature estimates with monthly CTD measurements between a depth of 0 and 50 m, the temperature at the depth of maximum primary productivity and the temperature at the chlorophyll maximum (Turich et al., 2013; http://www.imars.usf.edu/cariaco, last access: November 2018) (Fig. 10). During the upwelling season, temperatures are significantly lower due to the upward migration of isotherms, whereas during the non-upwelling period, temperatures are higher, particularly in the upper 20 m, and the water column is more stratified (Fig. 10). LDI underestimates the SST during stratification, which suggests that the LCD producers may thrive at depths of ca. 20–30 m. During upwelling, LDI temperatures agree better with SST, implying that the habitat of the LCD producers is potentially closer to the surface, coincident with the shoaling of the nutricline and thermocline (Fig. 10). However, these absolute differences in LDI temperatures are generally within the calibration error ($2\,°C$); thus, these seasonal variations in LDI temperatures should be interpreted with caution. Turich et al. (2003) found that the $U_{37}^{K'}$-derived temperatures agreed reasonably well with the measured temperatures at the chlorophyll maximum, which is generally found below a depth of 20 m (average depth of 30–34 m; ranging between 1 and 55 m) in the Cariaco Basin. The LDI temperatures are almost always higher than the temperatures at the chlorophyll maximum (Fig. 10), and higher than the temperatures at a depth of 30 m, implying that the LDI producers may reside in the upper 30 m of the water column; this is consistent with the results of Rampen et al. (2012) which showed that LDI-derived temperatures have the strongest correlation with the temperatures in the upper 20 m of the water column. This also agrees with Balzano et al. (2018) who observed the highest LCD abundances within the upper 20 m of the water column in the tropical Atlantic.

In the Mozambique Channel, the LDI temperature variations are much smaller ($< 2\,°C$; Fig. 7a) than the seasonal SST variation – ranging between ca. 24.5 and 30.5 °C. Accordingly, during the warmest months of the year, the difference between LDI-derived and satellite-derived SST is outside the calibration error (i.e., $> 2\,°C$). However, this is sim-

Figure 10. LDI temperature records for the Cariaco Basin time series May 1991–May 2000 and July 2002–July 2003 for Trap A (depth of 275 m; solid symbols) and Trap B (depth of 455 m; dashed symbols), with CTD-derived temperatures at depths of 2, 10, 20, 30 and 50 m (in red; http://www.imars.usf.edu/CAR/index.html, last access: November 2018; CARIACO time series composite CTD profiles), the temperature at the depth of maximum primary production (PP maximum; green) and the temperature at the depth of the chlorophyll maximum (yellow; data adapted from Turich et al., 2013). The shaded area represents the upwelling season.

ilar to the $U_{37}^{K'}$ and TEX_{86}^H which also did not reveal seasonal variations. This lack of seasonality was explained by the lateral advection and resuspension of fine sediment material by migrating mesoscale eddies which ending up in the deeply moored sediment trap (Fallet et al., 2011, 2012). Most likely, this also explains the lack of seasonal variation in our LDI record (Fig. 7a). Nevertheless, the average LDI temperature for the sediment trap of 26.4 °C agrees reasonably well with the annual mean satellite-derived SST of 27.6 °C for the sampled years. Additionally, there is a good agreement with the average LDI temperature of 26.0 °C for the two underlying surface sediments, as well as with the decadal average SST of 26.7 °C for 1955–2012 (Locarnini et al., 2013) given by the World Ocean Atlas (2013). For the North Atlantic, we also observe rather constant LDI temperatures during the year (Fig. 4) which contrasts with seasonal variations in satellite SSTs of ca. 3 to 5 °C. Nevertheless, differences

are mostly within the calibration error, except at M1 and M2 where LDI-derived temperatures are between 0.5 and 2.8 °C higher than satellite SSTs during winter and spring. Similar to the LDI, the TEX_{86}^H and $U_{37}^{K'}$-derived SSTs for the tropical Atlantic sediment traps also do not reveal clear seasonal variation. As all three proxies show minimal seasonal variability, this might indicate that the lipids are potentially allochtonous and partially derive from distant regions, resulting in an integrated average temperature signal, similar to the Mozambique Channel. Nevertheless, the flux-weighted annual LDI temperatures of the tropical Atlantic sediment traps (26.6 for M1 and 27.1 °C for M2 and M4) agree well with the annual mean satellite-derived SSTs of 26.1, 26.0 and 27.5 °C for M1, M2 and M4, respectively. Moreover, the LDI-derived temperatures in the underlying sediments (26.5, 26.6 and 26.7 °C, respectively) do not only agree well with those found in a single year in the sediment traps, but they also agree with the decadal average SSTs for 1955 to 2012 (26.2, 27.1 and 26.3 °C, respectively; Locarnini et al., 2013; Fig. 6a).

5 Conclusions

In this study we evaluated LCD-based proxies, particularly the LDI, in sediment trap time series from five sites in the tropical North Atlantic, the Cariaco Basin and the Mozambique Channel. For the North Atlantic we found that ca. 25 %–85 % of the export of these lipid biomarkers was preserved during settling from 1200 to 3500 m in the water column, and that generally less than 2 % was preserved in the surface sediments. Despite substantial degradation at the seafloor, likely linked to the prolonged oxygen exposure time, LCD-derived temperatures from the sediments are generally very similar to the annual mean LCD-derived temperatures in both the deep and shallow traps as well as to the annual mean SST for the specific sampling year and on decadal timescales for the specific sites. In the Cariaco Basin we observe a seasonal signal in the LDI linked to the upwelling season reflecting temperatures of the upper ca. 30 m of the water column. The LDI temperatures in the Mozambique Channel and the tropical Atlantic reveal minimal seasonal change although the seasonal SST contrasts amount to 3–5 °C. For the Mozambique Channel this is likely caused by the lateral advection of resuspended sediment by mesoscale eddy migration, a signal not substantially altered by diagenesis. Seasonal variations in the diol index are minimal in the central and western North Atlantic and 1,14-diol concentrations are rather low, implying little *Proboscia* diatom productivity. However, in the eastern Atlantic, closest to the African continent, the diol index attains a clear spring maximum that is likely associated with upwelling in the Guinea Dome during summer to autumn, suggesting the diol index reflects a pre-upwelling signal, consistent with the current knowledge on *Proboscia* ecology. In the Cariaco Basin, controlled by

seasonal upwelling, the diol index reveals the same clear seasonal trend observed in primary productivity, arguing that the diol index is an excellent indicator of upwelling intensity for this location.

Author contributions. MWdB, JSSD and SS designed the experiments, and MWdB carried them out. JU carried out the time series analysis. JBWS, GJAB and RCT deployed sediment traps and collected sediment trap materials. MWdB prepared the paper with contributions from all coauthors.

References

Araujo, M., Noriega, C., Hounsou-gbo, G. A., Veleda, D., Araujo, J., Bruto, L., Feitosa, F., Flores-Montes, M., Lefevre, N., Melo, P., Otsuka, A., Travassos, K., Schwamborn, R., and Neumann-Leitao, S.: A Synoptic Assessment of the Amazon River-Ocean Continuum during Boreal Autumn: From Physics to Plankton Communities and Carbon Flux, Front. Microbiol., 8, 1358, https://doi.org/10.3389/fmicb.2017.01358, 2017.

Balzano, S., Lattaud, J., Villanueva, L., Rampen, S. W., Brussaard, C. P. D., van Bleijswijk, J., Bale, N., Sinninghe Damsté, J. S., and Schouten, S.: A quest for the biological sources of long

chain alkyl diols in the western tropical North Atlantic Ocean, Biogeosciences, 15, 5951–5968, https://doi.org/10.5194/bg-15-5951-2018, 2018.

Biastoch, A. and Krauss, W.: The Role of Mesoscale Eddies in the Source Regions of the Agulhas Current, J. Phys. Oceanogr., 29, 2303–2317, https://doi.org/10.1175/1520-0485(1999)029<2303:Tromei>2.0.Co;2, 1999.

Bogus, K. A., Zonneveld, K. A. F., Fischer, D., Kasten, S., Bohrmann, G., and Versteegh, G. J. M.: The effect of meter-scale lateral oxygen gradients at the sediment-water interface on selected organic matter based alteration, productivity and temperature proxies, Biogeosciences, 9, 1553–1570, https://doi.org/10.5194/bg-9-1553-2012, 2012.

Brassell, S. C.: Climatic influences on the Paleogene evolution of alkenones, Paleoceanography, 29, 255–272, https://doi.org/10.1002/2013pa002576, 2014.

Brassell, S. C., Eglinton, G., Marlowe, I. T., Pflaumann, U., and Sarnthein, M.: Molecular stratigraphy – A new tool for climatic assessment, Nature, 320, 129–133, https://doi.org/10.1038/320129a0, 1986.

Chen, W. W., Mohtadi, M., Schefuss, E., and Mollenhauer, G.: Organic-geochemical proxies of sea surface temperature in surface sediments of the tropical eastern Indian Ocean, Deep-Sea Res. Pt. I, 88, 17–29, https://doi.org/10.1016/j.dsr.2014.03.005, 2014.

Coles, V. J., Brooks, M. T., Hopkins, J., Stukel, M. R., Yager, P. L., and Hood, R. R.: The pathways and properties of the Amazon River Plume in the tropical North Atlantic Ocean, J. Geophys. Res.-Oceans, 118, 6894–6913, https://doi.org/10.1002/2013jc008981, 2013.

Conte, M. H., Thompson, A., and Eglinton, G.: Primary production of lipid biomarker compounds by *Emiliania Huxleyi* – Results from an experimental mesocosm study in fjords of southwestern Norway, Sarsia, 79, 319–331, https://doi.org/10.1080/00364827.1994.10413564, 1994.

Conte, M. H., Weber, J. C., King, L. L., and Wakeham, S. G.: The alkenone temperature signal in western North Atlantic surface waters, Geochim. Cosmochim. Ac., 65, 4275–4287, 2001.

Conte, M. H., Sicre, M. A., Ruhlemann, C., Weber, J. C., Schulte, S., Schulz-Bull, D., and Blanz, T.: Global temperature calibration of the alkenone unsaturation index $U^{K'}_{37}$ in surface waters and comparison with surface sediments, Geochem. Geophy. Geosy., 7, Q02005, https://doi.org/10.1029/2005GC001054, 2006.

Cropper, T. E., Hanna, E., and Bigg, G. R.: Spatial and temporal seasonal trends in coastal upwelling off Northwest Africa, 1981–2012, Deep-Sea Res. Pt. I, 86, 94–111, https://doi.org/10.1016/j.dsr.2014.01.007, 2014.

Crosta, X., Romero, O. E., Ther, O., and Schneider, R. R.: Climatically-controlled siliceous productivity in the eastern Gulf of Guinea during the last 40 000 yr, Clim. Past, 8, 415–431, https://doi.org/10.5194/cp-8-415-2012, 2012.

de Bar, M. W., Dorhout, D. J. C., Hopmans, E. C., Rampen, S. W., Sinninghe Damsté, J. S., and Schouten, S.: Constraints on the application of long chain diol proxies in the Iberian Atlantic margin, Org. Geochem., 101, 184–195, https://doi.org/10.1016/j.orggeochem.2016.09.005, 2016.

de Bar, M. W., Ullgren, J., Thunell, R. C., Wakeham, S. G., Brummer, G.-J. A., Stuut, J.-B. W., Sinninghe Damsté, J. S., and Schouten, S.: Long chain diols in settling particles in tropi-

cal oceans: insights into sources, seasonality and proxies, PANGAEA, https://doi.org/10.1594/PANGAEA.898278, 2019.

de Jonge, C., Hopmans, E. C., Zell, C. I., Kim, J. H., Schouten, S., and Sinninghe Damsté, J. S.: Occurrence and abundance of 6-methyl branched glycerol dialkyl glycerol tetraethers in soils: Implications for palaeoclimate reconstruction, Geochim. Cosmochim. Ac., 141, 97–112, https://doi.org/10.1016/j.gca.2014.06.013, 2014.

de Jonge, C., Stadnitskaia, A., Hopmans, E. C., Cherkashov, G., Fedotov, A., Streletskaya, I. D., Vasiliev, A. A., and Sinninghe Damsté, J. S.: Drastic changes in the distribution of branched tetraether lipids in suspended matter and sediments from the Yenisei River and Kara Sea (Siberia): Implications for the use of brGDGT-based proxies in coastal marine sediments, Geochim. Cosmochim. Ac., 165, 200–225, https://doi.org/10.1016/j.gca.2015.05.044, 2015.

Doi, T., Tozuka, T., and Yamagata, T.: Interannual variability of the Guinea Dome and its possible link with the Atlantic Meridional Mode, Clim. Dynam., 33, 985–998, https://doi.org/10.1007/s00382-009-0574-z, 2009.

Duce, R. A., Liss, P. S., Merrill, J. T., Atlas, E. L Buat-Menard, P., Hicks, B. B., Miller, J. M., Prospero, J. M., Arimoto, R., Church, T. M., Ellis, W., Galloway, J. N., Hansen, L., Jickells, T. D., Knap, A. H., Reinhardt, K. H., Schneider, B., Soudine, A., Tokos, J. J., Tsunogai, S., Wollast, R., and Zhou, M.: The Atmospheric Input of Trace Species to the World Ocean, Global Biogeochem. Cy., 5, 193–259, https://doi.org/10.1029/91gb01778, 1991.

Fallet, U., Brummer, G. J., Zinke, J., Vogels, S., and Ridderinkhof, H.: Contrasting seasonal fluxes of planktonic foraminifera and impacts on paleothermometry in the Mozambique Channel upstream of the Agulhas Current, Paleoceanography, 25, PA4223, https://doi.org/10.1029/2010pa001942, 2010.

Fallet, U., Ullgren, J. E., Castaneda, I. S., van Aken, H. M., Schouten, S., Ridderinkhof, H., and Brummer, G. J. A.: Contrasting variability in foraminiferal and organic paleotemperature proxies in sedimenting particles of the Mozambique Channel (SW Indian Ocean), Geochim. Cosmochim. Ac., 75, 5834–5848, https://doi.org/10.1016/j.gca.2011.08.009, 2011.

Fallet, U., Castaneda, I. S., Aneurin, H. E., Richter, T. O., Boer, W., Schouten, S., and Brummer, G. J.: Sedimentation and burial of organic and inorganic temperature proxies in the Mozambique Channel, SW Indian Ocean, Deep-Sea Res. Pt. I, 59, 37–53, https://doi.org/10.1016/j.dsr.2011.10.002, 2012.

Ferreira, A. M., Miranda, A., Caetano, M., Baas, M., Vale, C., and Sinninghe Damsté, J. S.: Formation of mid-chain alkane keto-ols by post-depositional oxidation of mid-chain diols in Mediterranean sapropels, Org. Geochem., 32, 271–276, https://doi.org/10.1016/S0146-6380(00)00181-9, 2001.

Frouin, R., Franz, B. A., and Werdell, P. J.: The SeaWiFS PAR product, in: Algorithm Updates for the Fourth SeaWiFS Data Reprocessing, edited by: Hooker, S. B. and Firestone, E. R., NASA Tech. Memo. 2003–206892, Volume 22, 46–50, The SeaWiFS PAR product, NASA Goddard Space Flight Center, Greenbelt, Maryland, 2003.

Goddard Earth Sciences Data and Information Services Center: TRMM (TMPA-RT) Near Real-Time Precipitation L3 1 day 0.25 degree × 0.25 degree V7, Greenbelt, MD, Goddard Earth Sciences Data and Information Services Center (GES DISC), available at: http://disc.gsfc.nasa.gov/datacollection/

TRMM_3B42RT_Daily_7.html (last access: 16 April 2019), 2016.

Goñi, M. A., Woodworth, M. P., Aceves, H. L., Thunell, R. C., Tappa, E., Black, D., Müller-Karger, F., Astor, Y., and Varela, R.: Generation, transport, and preservation of the alkenone-based U^K_{37} sea surface temperature index in the water column and sediments of the Cariaco Basin (Venezuela), Global Biogeochem. Cy., 18, 1–21, https://doi.org/10.1029/2003GB002132, 2004.

Gordon, A. L.: Inter-ocean exchange of thermocline water, J. Geophys. Res.-Oceans, 91, 5037–5046, https://doi.org/10.1029/JC091iC04p05037, 1986.

Goudie, A. S. and Middleton, N. J.: Saharan dust storms: nature and consequences, Earth-Sci. Rev., 56, 179–204, https://doi.org/10.1016/S0012-8252(01)00067-8, 2001.

Guerreiro, C. V., Baumann, K.-H., Brummer, G.-J. A., Fischer, G., Korte, L. F., Merkel, U., Sá, C., de Stigter, H., and Stuut, J.-B. W.: Coccolithophore fluxes in the open tropical North Atlantic: influence of thermocline depth, Amazon water, and Saharan dust, Biogeosciences, 14, 4577–4599, https://doi.org/10.5194/bg-14-4577-2017, 2017.

Guerreiro, C. V., Baumann, K.-H., Brummer, G.-J. A., Fischer, G., Korte, L. F., Sá, C., and Stuut, J.-B. W.: Wind-forced transatlantic gradients in coccolithophore species fluxes, Prog. Oceanogr., in review, 2019.

Harlander, U., Ridderinkhof, H., Schouten, M. W., and de Ruijter, W. P. M.: Long-term observations of transport, eddies, and Rossby waves in the Mozambique Channel, J. Geophys. Res.-Oceans, 114, C02003, https://doi.org/10.1029/2008jc004846, 2009.

Hartnett, H. E., Keil, R. G., Hedges, J. I., and Devol, A. H.: Influence of oxygen exposure time on organic carbon preservation in continental margin sediments, Nature, 391, 572–574, https://doi.org/10.1038/35351, 1998.

Hedges, J. I., Sheng Hu, F., Devol, A. H., Hartnett, H. E., Tsamakis, E., and Keil, R. G.: Sedimentary organic matter preservation: a test for selective degradation under oxic conditions, Am. J. Sci., 299, 529–555, https://doi.org/10.2475/ajs.299.7-9.529 1999.

Herndl, G. J., Reinthaler, T., Teira, E., van Aken, H., Veth, C., Pernthaler, A., and Pernthaler, J.: Contribution of *Archaea* to total prokaryotic production in the deep Atlantic Ocean, Appl. Environ. Microb., 71, 2303–2309, https://doi.org/10.1128/aem.71.5.2303-2309.2005, 2005.

Honjo, S. and Doherty, K. W.: Large aperture time-series sediment traps; design objectives, construction and application, Deep-Sea Res., 35, 133–149, https://doi.org/10.1016/0198-0149(88)90062-3, 1988.

Hopmans, E. C., Weijers, J. W. H., Schefuß, E., Herfort, L., Sinninghe Damsté, J. S., and Schouten, S.: A novel proxy for terrestrial organic matter in sediments based on branched and isoprenoid tetraether lipids, Earth Planet. Sc. Lett., 224, 107–116, https://doi.org/10.1016/j.epsl.2004.05.012, 2004.

Hopmans, E. C., Schouten, S., and Sinninghe Damsté, J. S.: The effect of improved chromatography on GDGT-based palaeoproxies, Org. Geochem., 93, 1–6, https://doi.org/10.1016/j.orggeochem.2015.12.006, 2016.

Huffman, G. J., Adler, R. F., Bolvin, D. T., Gu, G., Nelkin, E. J., Bowman, K. P., Hong, Y., Stocker, E. F., and Wolff, D. B.: The TRMM Multi-satellite Precipitation Analysis: Quasi-Global, Multi-Year, Combined-Sensor Precipitation Estimates at Fine Scale, J. Hydrometeorol., 8, 38–55, https://doi.org/10.1175/JHM560.1, 2007.

Hughen, K. A., Overpeck, J. T., Peterson, L. C., and Anderson, R. F.: The nature of varved sedimentation in the Cariaco Basin, Venezuela, and its palaeoclimatic significance, Geol. Soc. Spec. Publ. London, 116, 171–183, https://doi.org/10.1144/gsl.Sp.1996.116.01.15, 1996.

Hughen, K. A., Overpeck, J. T., Lehman, S. J., Kashgarian, M., Southon, J., Peterson, L. C., Alley, R., and Sigman, D. M.: Deglacial changes in ocean circulation from an extended radiocarbon calibration, Nature, 391, 65–68, https://doi.org/10.1038/34150, 1998.

Huguet, C., Hopmans, E. C., Febo-Ayala, W., Thompson, D. H., Sinninghe Damsté, J. S., and Schouten, S.: An improved method to determine the absolute abundance of glycerol dibiphytanyl glycerol tetraether lipids, Org. Geochem., 37, 1036–1041, https://doi.org/10.1016/j.orggeochem.2006.05.008, 2006.

Huguet, C., Schimmelmann, A., Thunell, R., Lourens, L. J., Sinninghe Damsté, J. S., and Schouten, S.: A study of the TEX_{86} paleothermometer in the water column and sediments of the Santa Barbara Basin, California, Paleoceanography, 22, PA3203, https://doi.org/10.1029/2006pa001310, 2007.

Jiang, S., O'Leary, T., Volkman, J. K., Zhang, H., Jia, R., Yu, S., Wang, Y., Luan, Z., Sun, Z., and Jiang, R.: Origins and simulated thermal alteration of sterols and keto-alcohols in deep-sea marine-sediments of the Okinawa Trough, Org. Geochem., 21, 415–422, https://doi.org/10.1016/0146-6380(94)90203-8, 1994.

Jonas, A. S., Schwark, L., and Bauersachs, T.: Late Quaternary water temperature variations of the Northwest Pacific based on the lipid paleothermometers TEX^H_{86}, $U^{K'}_{37}$ and LDI, Deep-Sea Res. Pt. I, 125, 81–93, https://doi.org/10.1016/j.dsr.2017.04.018, 2017.

Karner, M. B., DeLong, E. F., and Karl, D. M.: Archaeal dominance in the mesopelagic zone of the Pacific Ocean, Nature, 409, 507–510, https://doi.org/10.1038/35054051, 2001.

Kim, J.-H., van der Meer, J., Schouten, S., Helmke, P., Willmott, V., Sangiorgi, F., Koc, N., Hopmans, E. C., and Sinninghe Damsté, J. S.: New indices and calibrations derived from the distribution of crenarchaeal isoprenoid tetraether lipids: Implications for past sea surface temperature reconstructions, Geochim. Cosmochim. Ac., 74, 4639–4654, https://doi.org/10.1016/j.gca.2010.05.027, 2010.

Kim, J.-H., Romero, O. E., Lohmann, G., Donner, B., Laepple, T., Haam, E., and Sinninghe Damsté, J. S.: Pronounced subsurface cooling of North Atlantic waters off Northwest Africa during Dansgaard–Oeschger interstadials, Earth Planet. Sc. Lett., 339–340, 95–102, https://doi.org/10.1016/j.epsl.2012.05.018, 2012.

Kim, J.-H., Schouten, S., Rodrigo-Gámiz, M., Rampen, S., Marino, G., Huguet, C., Helmke, P., Buscail, R., Hopmans, E. C., Pross, J., Sangiorgi, F., Middelburg, J. B. M., and Sinninghe Damsté, J. S.: Influence of deep-water derived isoprenoid tetraether lipids on the TEX^H_{86} paleothermometer in the Mediterranean Sea, Geochim. Cosmochim. Ac., 150, 125–141, https://doi.org/10.1016/j.gca.2014.11.017, 2015.

Koning, E., van Iperen, J. M., van Raaphorst, W., Helder, W., Brummer, G.-J. A., and van Weering, T. C. E.: Selective preservation of upwelling-indicating diatoms in sediments off Somalia, NW Indian Ocean, Deep-Sea Res. Pt. I, 48, 2473–2495, https://doi.org/10.1016/S0967-0637(01)00019-X, 2001.

Korte, L. F., Brummer, G.-J. A., van der Does, M., Guerreiro, C. V., Hennekam, R., van Hateren, J. A., Jong, D., Munday, C. I., Schouten, S., and Stuut, J.-B. W.: Downward particle fluxes of biogenic matter and Saharan dust across the equatorial North Atlantic, Atmos. Chem. Phys., 17, 6023–6040, https://doi.org/10.5194/acp-17-6023-2017, 2017.

Lange, C. B., Romero, O. E., Wefer, G., and Gabric, A. J.: Offshore influence of coastal upwelling off Mauritania, NW Africa, as recorded by diatoms in sediment traps at 2195 m water depth, Deep-Sea Res. Pt. I, 45, 986–1013, https://doi.org/10.1016/s0967-0637(97)00103-9 1998.

Lattaud, J., Kim, J.-H., De Jonge, C., Zell, C., Sinninghe Damsté, J. S., and Schouten, S.: The C_{32} alkane-1,15-diol as a tracer for riverine input in coastal seas, Geochim. Cosmochim. Ac., 202, 146–158, https://doi.org/10.1016/j.gca.2016.12.030, 2017a.

Lattaud, J., Dorhout, D., Schulz, H., Castañeda, I. S., Schefuß, E., Sinninghe Damsté, J. S., and Schouten, S.: The C_{32} alkane-1,15-diol as a proxy of late Quaternary riverine input in coastal margins, Clim. Past, 13, 1049–1061, https://doi.org/10.5194/cp-13-1049-2017, 2017b.

Lee, T., Lagerloef, G., Gierach, M. M., Kao, H.-Y., Yueh, S., and Dohan, K.: Aquarius reveals salinity structure of tropical instability waves, Geophys. Res. Lett., 39, L12610, https://doi.org/10.1029/2012GL052232, 2012.

Lefèvre, N., Moore, G., Aiken, J., Watson, A., and Cooper, D.: Variability of pCO_2 in the tropical Atlantic in 1995, J. Geophys. Res., C3, 5623–5634, https://doi.org/10.1029/97JC02303, 1998.

Locarnini, R. A., Mishonov, A. V., Antonov, J. I., Boyer, T. P., Garcia, H. E., Baranova, O. K., Zweng, M. M., Paver, C. R., Reagan, J. R., Johnson, D. R., Hamilton, M., and Seidov, D.: World Ocean Atlas 2013, in: Volume 1: temperature, Technical Ed., NOAA Atlas NESDIS 73, 40 pp., Levitus S, Silver Spring, 2013.

Lopes dos Santos, R. A., Prange, M., Castañeda, I. S., Schefuß, E., Mulitza, S., Schulz, M., Niedermeyer, E. M., Sinninghe Damsté, J. S., and Schouten, S.: Glacial-interglacial variability in Atlantic meridional overturning circulation and thermocline adjustments in the tropical North Atlantic, Earth Planet. Sc. Lett., 300, 407–414, https://doi.org/10.1016/j.epsl.2010.10.030, 2010.

Lopes dos Santos, R. A. L., Spooner, M. I., Barrows, T. T., De Deckker, P., Sinninghe Damsté, J. S., and Schouten, S.: Comparison of organic ($U_{37}^{K'}$, TEX_{86}^{H}, LDI) and faunal proxies (foraminiferal assemblages) for reconstruction of late Quaternary sea surface temperature variability from offshore southeastern Australia, Paleoceanography, 28, 377–387, https://doi.org/10.1002/palo.20035, 2013.

Lutjeharms, J. R. E.: The Agulhas Current, 330 pp., Springer, Berlin, 2006.

Malauene, B. S., Shillington, F. A., Roberts, M. J., and Moloney, C. L.: Cool, elevated chlorophyll-a waters off northern Mozambique, Deep-Sea Res. Pt. II, 100, 68–78, https://doi.org/10.1016/j.dsr2.2013.10.017, 2014.

Marlowe, I. T., Green, J. C., Neal, A. C., Brassell, S. C., Eglinton, G., and Course, P. A.: Long-Chain (n-C_{37}–C_{39}) alkenones in the Prymnesiophyceae. Distribution of alkenones and other lipids and their taxonomic significance, Brit. Phycol. J., 19, 203–216, https://doi.org/10.1080/00071618400650221, 1984.

Martin, J. H. and Fitzwater, S. E.: Iron-deficiency limits phytoplankton growth in the Northeast Pacific Subarctic, Nature, 331, 341–343, https://doi.org/10.1038/331341a0, 1988.

Mazeika, P. A.: Thermal domes in the Eastern Tropical Atlantic Ocean, Limnol. Oceanogr., 12, 537–539, https://doi.org/10.4319/lo.1967.12.3.0537, 1967.

Méjanelle, L., Sanchez-Gargallo, A., Bentaleb, I., and Grimalt, J. O.: Long chain n-alkyl diols, hydroxy ketones and sterols in a marine eustigmatophyte, *Nannochloropsis gaditana*, and in *Brachionus plicatilis* feeding on the algae, Org. Geochem., 34, 527–538, https://doi.org/10.1016/s0146-6380(02)00246-2, 2003.

Müller, P. J. and Fischer, G.: A 4-year sediment trap record of alkenones from the filamentous upwelling region off Cape Blanc, NW Africa and a comparison with distributions in underlying sediments, Deep-Sea Res. Pt. I, 48, 1877–1903, https://doi.org/10.1016/S0967-0637(00)00109-6, 2001.

Müller, P. J., Kirst, G., Ruhland, G., von Storch, I., and Rosell-Melé, A.: Calibration of the alkenone paleotemperature index $U_{37}^{K'}$ based on core-tops from the eastern South Atlantic and the global ocean (60° N–60° S), Geochim. Cosmochim. Ac., 62, 1757–1772, https://doi.org/10.1016/s0016-7037(98)00097-0, 1998.

Müller-Karger, F. E., McClain, C. R., and Richardson, P. L.: The dispersal of the Amazon's water, Nature, 333, 56–59, https://doi.org/10.1038/333056a0, 1988.

Müller-Karger, F. E., Richardson, P. L., and McGillicuddy, D.: On the offshore dispersal of the Amazon's Plume in the North Atlantic: Comments on the paper by A. Longhurst, "Seasonal cooling and blooming in tropical oceans", Deep-Sea Res. Pt. I, 42, 2127–2137, https://doi.org/10.1016/0967-0637(95)00085-2, 1995.

Müller-Karger, F., Varela, R., Thunell, R., Scranton, M., Bohrer, R., Taylor, G., Capelo, J., Astor, Y., Tappa, E., Ho, T. Y., and Walsh, J. J.: Annual cycle of primary production in the Cariaco Basin: Response to upwelling and implications for vertical export, J. Geophys. Res., 106, 4527–4542, https://doi.org/10.1029/1999JC000291, 2001.

Müller-Karger, F., Varela, R., Thunell, R., Astor, Y., Zhang, H. Y., Luerssen, R., and Hu, C. M.: Processes of coastal upwelling and carbon flux in the Cariaco Basin, Deep-Sea Res. Pt. II, 51, 927–943, https://doi.org/10.1016/j.dsr2.2003.10.010, 2004.

Naafs, B. D. A., Hefter, J., and Stein, R.: Application of the long chain diol index (LDI) paleothermometer to the early Pleistocene (MIS 96), Org. Geochem., 49, 83–85, https://doi.org/10.1016/j.orggeochem.2012.05.011, 2012.

NASA Aquarius project: Aquarius Official Release Level 3 Sea Surface Salinity Standard Mapped Image Daily Data V4.0. Ver. 4.0. PO.DAAC, CA, USA, 2015a.

NASA Aquarius project: Aquarius Official Release Level 3 Wind Speed Standard Mapped Image Daily Data V4.0. Ver. 4.0. PO.DAAC, CA, USA, 2015b.

Nehring, D., Hagen, E., Jorge da Silva, A., Schemainda, R., Wolf, G., Michelchen, N., Kaiser, W., Postel, L., Gosselk, F., and Brenning, U.: The oceanological conditions in the western part of the Mozambique Channel in February–March 1980, Nationalkomitee für Geodäsie und Geophysik bei der Akademie der Wissenschaften der DDR, Potsdam, Germany, 1984.

Peeters, F. J. C., Acheson, R., Brummer, G. J. A., de Ruijter, W. P. M., Schneider, R. R., Ganssen, G. M., Ufkes, E., and Kroon, D.: Vigorous exchange between the Indian and Atlantic oceans at the end of the past five glacial periods, Nature, 430, 661–665, https://doi.org/10.1038/nature02785, 2004.

Peterson, L. C., Overpeck, J. T., Kipp, N. G., and Imbrie, J.: A high-resolution Late Quaternary upwelling record from the anoxic Cariaco Basin, Venezuela, Paleoceanography, 6, 99–119, https://doi.org/10.1029/90pa02497, 1991.

Prahl, F. G. and Wakeham, S. G.: Calibration of unsaturation patterns in long-chain ketone compositions for paleotemperature assessment, Nature, 330, 367–369, https://doi.org/10.1038/330367a0, 1987.

Prahl, F. G., Dymond, J., and Sparrow, M. A.: Annual biomarker record for export production in the central Arabian Sea, Deep-Sea Res. Pt. II, 47, 1581–1604, https://doi.org/10.1016/S0967-0645(99)00155-1, 2000.

Rampen, S. W., Schouten, S., Wakeham, S. G., and Sinninghe Damsté, J. S.: Seasonal and spatial variation in the sources and fluxes of long chain diols and mid-chain hydroxy methyl alkanoates in the Arabian Sea, Org. Geochem., 38, 165–179, https://doi.org/10.1016/j.orggeochem.2006.10.008, 2007.

Rampen, S. W., Schouten, S., Koning, E., Brummer, G.-J. A., and Sinninghe Damsté, J. S.: A 90 kyr upwelling record from the northwestern Indian Ocean using a novel long-chain diol index, Earth Planet. Sc. Lett., 276, 207–213, https://doi.org/10.1016/j.epsl.2008.09.022, 2008.

Rampen, S. W., Schouten, S., and Sinninghe Damsté, J. S.: Occurrence of long chain 1,14-diols in *Apedinella radians*, Org. Geochem., 42, 572–574, https://doi.org/10.1016/j.orggeochem.2011.03.009, 2011.

Rampen, S. W., Willmott, V., Kim, J. H., Uliana, E., Mollenhauer, G., Schefuss, E., Sinninghe Damsté, J. S., and Schouten, S.: Long chain 1,13-and 1,15-diols as a potential proxy for palaeotemperature reconstruction, Geochim. Cosmochim. Ac., 84, 204–216, https://doi.org/10.1016/j.gca.2012.01.024, 2012.

Rampen, S. W., Willmott, V., Kim, J. H., Rodrigo-Gámiz, M., Uliana, E., Mollenhauer, G., Schefuss, E., Sinninghe Damsté, J. S., and Schouten, S.: Evaluation of long chain 1,14-alkyl diols in marine sediments as indicators for upwelling and temperature, Org. Geochem., 76, 39–47, https://doi.org/10.1016/j.orggeochem.2014.07.012, 2014a.

Rampen, S. W., Datema, M., Rodrigo-Gámiz, M., Schouten, S., Reichart, G. J., and Sinninghe Damsté, J. S.: Sources and proxy potential of long chain alkyl diols in lacustrine environments, Geochim. Cosmochim. Ac., 144, 59–71, https://doi.org/10.1016/j.gca.2014.08.033, 2014b.

Reiche, S., Rampen, S. W., Dorhout, D. J. C., Sinninghe Damsté, J. S., and Schouten, S.: The impact of oxygen exposure on long-chain alkyl diols and the long chain diol index (LDI) – a long-term incubation study, Org. Geochem., 124, 238–246, https://doi.org/10.1016/j.orggeochem.2018.08.003, 2018.

Richards, F. A.: The Cariaco Basin (Trench), Oceanogr. Mar. Biol., 13, 11–67, 1975.

Richardson, P. L. and Reverdin, G.: Seasonal cycle of velocity in the Atlantic North Equatorial Countercurrent as measured by surface drifters, current meters, and ship drifts, J. Geophys. Res.-Oceans, 92, 3691–3708, https://doi.org/10.1029/JC092iC04p03691, 1987.

Ridderinkhof, H., van der Werf, P. M., Ullgren, J. E., van Aken, H. M., van Leeuwen, P. J., and de Ruijter, W. P. M.: Seasonal and interannual variability in the Mozambique Channel from moored current observations, J. Geophys. Res.-Oceans, 115, C06010, https://doi.org/10.1029/2009jc005619, 2010.

Rodrigo-Gámiz, M., Rampen, S. W., de Haas, H., Baas, M., Schouten, S., and Sinninghe Damsté, J. S.: Constraints on the applicability of the organic temperature proxies $U^{K'}_{37}$, TEX$_{86}$ and LDI in the subpolar region around Iceland, Biogeosciences, 12, 6573–6590, https://doi.org/10.5194/bg-12-6573-2015, 2015.

Rodrigo-Gámiz, M., Rampen, S. W., Schouten, S., and Sinninghe Damsté, J. S.: The impact of oxic degradation on long chain alkyl diol distributions in Arabian Sea surface sediments, Org. Geochem., 100, 1–9, https://doi.org/10.1016/j.orggeochem.2016.07.003, 2016.

Romero O. E., Lange C. B., Fischer G., Treppke U. F., and Wefer G.: Variability in Export Production Documented by Downward Fluxes and Species Composition of Marine Planktic Diatoms: Observations from the Tropical and Equatorial Atlantic, in: Use of Proxies in Paleoceanography, edited by: Fischer, G. and Wefer, G., Springer, Berlin, Heidelberg, 1999.

Rosell-Melé, A. and Prahl, F. G.: Seasonality of $U^{K'}_{37}$ temperature estimates as inferred from sediment trap data, Quaternary Sci. Rev., 72, 128–136, https://doi.org/10.1016/j.quascirev.2013.04.017, 2013.

Rossignol, M. and Meyruis, A. M.: Campagnes océanographiques du Gérard-Tréca, 53 pp., Cent. Oceanogr. Dakar-Thiaroye, ORSTOM, Dakar, Senegal, 1964.

Sætre, R. and Da Silva, A. J.: The circulation of the Mozambique channel, Deep-Sea Res., 31, 485–508, https://doi.org/10.1016/0198-0149(84)90098-0, 1984.

Schlitzer, R.: Data Analysis and Visualization with Ocean Data View, CMOS Bulletin SCMO, 43, 9–13, available at: https://odv.awi.de/ (last access: March 2019), 2015.

Schouten, M. W., de Ruijter, W. P. M., van Leeuwen, P. J., and Ridderinkhof, H.: Eddies and variability in the Mozambique Channel, Deep-Sea Res. Pt. II, 50, 1987–2003, https://doi.org/10.1016/s0967-0645(03)00042-0, 2003.

Schouten, S., Hopmans, E. C., Schefuss, E., and Sinninghe Damsté, J. S.: Distributional variations in marine crenarchaeotal membrane lipids: a new tool for reconstructing ancient sea water temperatures?, Earth Planet. Sc. Lett., 204, 265–274, https://doi.org/10.1016/s0012-821x(02)00979-2, 2002.

Schouten, S., Hopmans, E. C., and Sinninghe Damsté, J. S.: The organic geochemistry of glycerol dialkyl glycerol tetraether lipids: A review, Org. Geochem., 54, 19–61, https://doi.org/10.1016/j.orggeochem.2012.09.006, 2013.

Schreuder, L. T., Stuut, J.-B. W., Korte, L. F., Sinninghe Damsté, J. S., and Schouten, S.: Aeolian transport and deposition of plant wax *n*-alkanes across the tropical North Atlantic Ocean, Org. Geochem., 115, 113–123, https://doi.org/10.1016/j.orggeochem.2017.10.010, 2018a.

Schreuder, L. T., Hopmans, E. C., Stuut, J.-B. W., Sinninghe Damsté, J. S., and Schouten, S.: Transport and deposition of the fire biomarker levoglucosan across the tropical North Atlantic Ocean, Geochim. Cosmochim. Ac., 227, 171–185, https://doi.org/10.1016/j.gca.2018.02.020, 2018b.

Sicre, M., Bard, E., Ezat, U., and Rostek, F.: Alkenone distributions in the North Atlantic and Nordic sea surface waters, Geochem. Geophy. Geosy., 3, 1013, https://doi.org/10.1029/2001GC000159, 2002.

Siedler, G., Zangenberg, N., and Onken, R.: Seasonal Changes in the Tropical Atlantic Circulation – Observation and Simulation

of the Guinea Dome, J. Geophys. Res.-Oceans, 97, 703–715, https://doi.org/10.1029/91jc02501, 1992.

Sinninghe Damsté, J. S., Rijpstra, W. I. C., Hopmans, E. C., Prahl, F. G., Wakeham, S. G., and Schouten, S.: Distribution of membrane lipids of planktonic Crenarchaeota in the Arabian seat, Appl. Environ. Microbiol., 68, 2997–3002, https://doi.org/10.1128/aem.68.6.2997-3002.2002, 2002.

Sinninghe Damsté, J. S., Rijpstra, W. I. C., and Reichart, G.-J.: The influence of oxic degradation on the sedimentary biomarker record II. Evidence from Arabian Sea sediments, Geochim. Cosmochim. Ac., 66, 2737–2754, https://doi.org/10.1016/S0016-7037(02)00865-7, 2002.

Sinninghe Damsté, J. S., Rampen, S., Rijpstra, W. I. C., Abbas, B., Muyzer, G., and Schouten, S.: A diatomaceous origin for long-chain diols and mid-chain hydroxy methyl alkanoates widely occurring in Quaternary marine sediments: Indicators for high-nutrient conditions, Geochim. Cosmochim. Ac., 67, 1339–1348, https://doi.org/10.1016/s0016-7037(02)01225-5, 2003.

Sinninghe Damsté, J. S., Rijpstra, W. I. C., Hopmans, E. C., den Uijl, M. J., Weijers, J. W. H., and Schouten, S.: The enigmatic structure of the crenarchaeol isomer, Org. Geochem., 124, 22–28, https://doi.org/10.1016/j.orggeochem.2018.06.005, 2018.

Smith, S. L.: Understanding the Arabian Sea: Reflections on the 1994–1996 Arabian Sea Expedition, Deep-Sea Res. Pt. II, 48, 1385–1402, https://doi.org/10.1016/S0967-0645(00)00144-2, 2001.

Stramma, L. and Schott, F.: The mean flow field of the tropical Atlantic Ocean, Deep-Sea Res. Pt. II, 46, 279–303, https://doi.org/10.1016/s0967-0645(98)00109-x, 1999.

Stuut, J.-B., Zabel, M., Ratmeyer, V., Helmke, P., Schefuß, E., Lavik, G., and Schneider, R.: Provenance of present-day eolian dust collected off NW Africa, J. Geophys. Res.-Atmos., 110, D04202, https://doi.org/10.1029/2004JD005161, 2005.

Thunell, R., Benitez-Nelson, C., Varela, R., Astor, Y., and Müller-Karger, F.: Particulate organic carbon fluxes along upwelling-dominated continental margins: Rates and mechanisms, Global Biogeochem. Cy., 21, GB1022, https://doi.org/10.1029/2006gb002793, 2007.

Thunell, R. C., Varela, R., Llano, M., Collister, J., Müller-Karger, F., and Bohrer, R.: Organic carbon fluxes, degradation, and accumulation in an anoxic basin: Sediment trap results from the Cariaco Basin, Limnol. Oceanogr., 45, 300–308, https://doi.org/10.4319/lo.2000.45.2.0300, 2000.

Tierney, J. E.: 12.14 – Biomarker-Based Inferences of Past Climate: The TEX_{86} Paleotemperature Proxy A2 – Holland, Heinrich D, in: Treatise on Geochemistry, 2nd Edn., edited by: Turekian, K. K., Elsevier, Oxford, 379–393, 2014.

Tierney, J. E. and Tingley, M. P.: A Bayesian, spatially-varying calibration model for the TEX_{86} proxy, Geochim. Cosmochim. Ac., 127, 83–106, https://doi.org/10.1016/j.gca.2013.11.026, 2014.

Tierney, J. E. and Tingley, M. P.: A TEX_{86} surface sediment database and extended Bayesian calibration, Scientific Data, 2, 150029, https://doi.org/10.1038/sdata.2015.29, 2015.

Tierney, J. E. and Tingley, M. P.: BAYSPLINE: A New Calibration for the Alkenone Paleothermometer, Paleoceanogr. Paleocl., 33, 281–301, https://doi.org/10.1002/2017pa003201, 2018.

Tierney, J. E., Sinninghe Damsté, J. S., Pancost, R. D., Sluijs, A., and Zachos, J. C.: Eocene temperature gradients, Nat. Geosci., 10, 538–539, https://doi.org/10.1038/ngeo2997, 2017.

Treppke, U. F., Lange, C. B., and Wefer, G.: Vertical fluxes of diatoms and silicoflagellates in the eastern equatorial Atlantic, and their contribution to the sedimentary record, Mar. Micropaleontol., 28, 73–96, https://doi.org/10.1016/0377-8398(95)00046-1, 1996.

Turich, C., Schouten, S., Thunell, R. C., Varela, R., Astor, Y., and Wakeham, S. G.: Comparison of TEX_{86} and $U^{K'}_{37}$ temperature proxies in sinking particles in the Cariaco Basin, Deep-Sea Res. Pt. I, 78, 115–133, https://doi.org/10.1016/j.dsr.2013.02.008, 2013.

Ullgren, J. E., van Aken, H. M., Ridderinkhof, H., and de Ruijter, W. P. M.: The hydrography of the Mozambique Channel from six years of continuous temperature, salinity, and velocity observations, Deep-Sea Res. Pt. I, 69, 36–50, https://doi.org/10.1016/j.dsr.2012.07.003, 2012.

van der Does, M., Korte, L. F., Munday, C. I., Brummer, G.-J. A., and Stuut, J.-B. W.: Particle size traces modern Saharan dust transport and deposition across the equatorial North Atlantic, Atmos. Chem. Phys., 16, 13697–13710, https://doi.org/10.5194/acp-16-13697-2016, 2016.

Versteegh, G. J. M., Bosch, H. J., and de Leeuw, J. W.: Potential palaeoenvironmental information of C_{24} to C_{36} mid-chain diols, keto-ols and mid-chain hydroxy fatty acids; a critical review, Org. Geochem., 27, 1–13, https://doi.org/10.1016/s0146-6380(97)00063-6, 1997.

Versteegh, G. J. M., Jansen, J. H. F., de Leeuw, J. W., and Schneider, R. R.: Mid-chain diols and keto-ols in SE Atlantic sediments: a new tool for tracing past sea surface water masses?, Geochim. Cosmochim. Ac., 64, 1879–1892, https://doi.org/10.1016/S0016-7037(99)00398-1, 2000.

Villanueva, L., Besseling, M., Rodrigo-Gámiz, M., Rampen, S. W., Verschuren, D., and Sinninghe Damsté, J. S.: Potential biological sources of long chain alkyl diols in a lacustrine system, Org. Geochem., 68, 27–30, https://doi.org/10.1016/j.orggeochem.2014.01.001, 2014.

Voituriez, B.: Les sous-courants equatoriaux nord et sud et la formation des dômes thermiques tropicaux, Oceanol. Acta, 4, 497–506, 1981.

Volkman, J. K., Eglinton, G., Corner, E. D. S., and Sargent, J. R.: Novel unsaturated straight-chain C_{37}-C_{39} methyl and ethyl ketones in marine sediments and a coccolithophore *Emiliania huxleyi*, Phys. Chem. Earth, 12, 219–227, https://doi.org/10.1016/0079-1946(79)90106-X, 1980.

Volkman, J. K., Barrett, S. M., Dunstan, G. A., and Jeffrey, S. W.: C_{30}–C_{32} alky diols and unsaturated alcohols in microalgae of the class Eustigmatophyceae, Org. Geochem., 18, 131–138, https://doi.org/10.1016/0146-6380(92)90150-v, 1992.

Volkman, J. K., Barrett, S. M., Blackburn, S. I., and Sikes, E. L.: Alkenones in *Gephyrocapsa Oceanica* – Implications for studies of paleoclimate, Geochim. Cosmochim. Ac., 59, 513–520, https://doi.org/10.1016/0016-7037(95)00325-t, 1995.

Volkman, J. K., Barrett, S. M., and Blackburn, S. I.: Eustigmatophyte microalgae are potential sources of C_{29} sterols, C_{22}–C_{28} *n*-alcohols and C_{28}–C_{32} *n*-alkyl diols in freshwater environments, Org. Geochem., 30, 307–318, https://doi.org/10.1016/s0146-6380(99)00009-1, 1999.

Wakeham, S. G., Peterson, M. L., Hedges, J. I., and Lee, C.: Lipid biomarker fluxes in the Arabian Sea, with a comparison to the

equatorial Pacific Ocean, Deep-Sea Res. Pt. II, 49, 2265–2301, https://doi.org/10.1016/S0967-0645(02)00037-1, 2002.

Warnock, J. P., Bauersachs, T., Kotthoff, U., Brandt, H. T., and Andren, E.: Holocene environmental history of the Angermanalven Estuary, northern Baltic Sea, Boreas, 47, 593–608, https://doi.org/10.1111/bor.12281, 2018.

Weijer, W., de Ruiter, W. P. M., Dijkstra, H. A., and van Leeuwen, P. J.: Impact of interbasin exchange on the Atlantic overturning circulation, J. Phys. Oceanogr., 29, 2266–2284, https://doi.org/10.1175/1520-0485(1999)029<2266:Ioieot>2.0.Co;2, 1999.

Willmott, V., Rampen, S. W., Domack, E., Canals, M., Sinninghe Damsté, J. S., and Schouten, S.: Holocene changes in Proboscia diatom productivity in shelf waters of the north-western Antarctic Peninsula, Antarct. Sci., 22, 3–10, https://doi.org/10.1017/s095410200999037x, 2010.

Wuchter, C., Schouten, S., Wakeham, S. G., and Sinninghe Damsté, J. S.: Temporal and spatial variation in tetraether membrane lipids of marine Crenarchaeota in particulate organic matter: Implications for TEX_{86} paleothermometry, Paleoceanography, 20, PA3013, https://doi.org/10.1029/2004pa001110, 2005.

Wuchter, C., Schouten, S., Wakeham, S. G., and Sinninghe Damsté, J. S.: Archaeal tetraether membrane lipid fluxes in the northeastern Pacific and the Arabian Sea: Implications for TEX_{86} paleothermometry, Paleoceanography, 21, PA4208, https://doi.org/10.1029/2006PA001279, 2006.

Xie, P. and Arkin, P. A.: Global precipitation: A 17-year monthly analysis based on gauge observations, satellite estimates, and numerical model outputs, B. Am. Meteorol. Soc., 78, 2539–2558, https://doi.org/10.1175/1520-0477(1997)078<2539:GPAYMA>2.0.CO;2, 1997.

Yamagata, T. and Iizuka, S.: Simulation of the Tropical Thermal Domes in the Atlantic – A Seasonal Cycle, J. Phys. Oceanogr., 25, 2129–2140, https://doi.org/10.1175/1520-0485(1995)025<2129:Sotttd>2.0.Co;2, 1995.

Yamamoto, M., Shimamoto, A., Fukuhara, T., Tanaka, Y., and Ishizaka, J.: Glycerol dialkyl glycerol tetraethers and TEX_{86} index in sinking particles in the western North Pacific, Org. Geochem., 53, 52–62, https://doi.org/10.1016/j.orggeochem.2012.04.010, 2012.

Zhang, Y. G. and Liu, X. Q.: Export Depth of the TEX_{86} Signal, Paleoceanogr. Paleocl., 33, 666–671, https://doi.org/10.1029/2018PA003337, 2018.